Mathematisches Forschungsinstitut Oberwolfach

Report No. 24/2009

DOI: 10.4171/OWR/2009/24

Mathematical Biology

Organised by
Emmanuele DiBenedetto, Nashville
Benoit Perthame, Paris
Angela Stevens, Heidelberg

May 3rd – May 9th, 2009

Abstract. Mathematical biology is a fast growing field of research, which on one hand side faces challenges resulting from the enormous amount of data provided by experimentalists in the recent years, on the other hand new mathematical methods may have to be developed to meet the demand for explanation and prediction on how specific biological systems function.

Mathematics Subject Classification (2000): 35B, 92C.

Introduction by the Organisers

The workshop *Mathematical Biology*, organized by Emmanuele DiBenedetto (Nashville), Benoit Perthame (Paris), and Angela Stevens (Heidelberg) was held May 3rd - May 9th, 2009. The Oberwolfach Institute was nearly fully occupied. Especially many young scientists took part in the meeting. Experimentalists, mathematical biologists, and mathematicians contributed to the lively discussions during the workshop.

The first day was devoted to presentations by experimentalists and by mathematicians, who closely collaborate with experimentalists.
Experiments for cell-cell signaling and chemotactic movement during the developmental life-cycle of the model organism *Dictyostelium discoideum* were discussed and during gastrulation of chicken embryos. Further, three-dimensional in vitro tissue spheroids as bio-medical model systems for real-time testing of active pharmaceutical ingredients were presented. Next, mathematical models for cell motility and self-organization, robustness of pattern formation during development, structured population models for stem cell renewal and differentiation, chemical kinetic models for the lac and the tryptophan operon, and models for the self assembly of

biomembranes were addressed.

Tuesday morning was devoted to multiscale models for tissue growth and tissue mechanics, as well as the mechanics of cell migration. In the afternoon stage structured population models for Leukemia were discussed, the effects of intracellular noise on quorum sensing, and an overview over cell-based morphogenetic models was given.

Since mathematical modeling of chemotaxis is a very fast developing field with still a number of mathematical challenges, a full morning session was dedicated to this topic. Models for multi-species chemotaxis, measure valued solutions for the classical Keller-Segel model and the continuation of solutions beyond blow-up were addressed, as well as pattern formation for chemotaxis models with non-diffusive memory. In this context also a kinetic model for swarming was presented.

The Thursday session mainly dealt with structured population models in a variety of contexts and related delay equations, which again was the topic of the very last presentation of the workshop. Thus these talks connected back to the earlier presentations on mathematical models for stem cells and leukemia. Further, during the day, examples for model supported data analysis were given, models which describe motor proteins moving along molecular filaments, numerical models for tumor growth, and a mathematical analysis of the random reorientation and movement of *Azospirillum brasilense* was presented.

The last day was devoted to to traveling waves in population dynamics. and deterministic and stochastic aspects of recombination.

Overall the workshop addressed mathematically challenging topics in the life-sciences, like age/stage structured population models, chemotaxis, and bio-mechanical models, as well as bio-medical experiments of actual interest. It was a pleasure for us to organize this workshop, and we are very grateful for the professional and very kind support of the Oberwolfach team before and during our stay at MFO.

Workshop: Mathematical Biology

Table of Contents

Abstracts

Analysis of cell-cell signalling and chemotactic movement during Dictyostelium development and chick gastrulation

Cornelis J. Weijer

We investigate the molecular mechanisms by which cells produce and detect chemotactic signals and translate this information in directed coordinated movement up or down chemical gradients. We study these questions in two different experimental systems, the social amoebae *Dictyostelium discoideu*, and during gastrulation in the chick embryo.

In Dictyostelium starvation for food induces the aggregation of thousands of individual amoebae into a multi-cellular aggregate. During aggregation the cells differentiate into a number of distinct celltypes, which form a migrating slug that transforms into a fruiting body consisting of a stalk supporting a mass of spores. The chemotactic aggregation of the cells is controlled by propagating waves of cyclic-AMP emanating periodically form aggregation centres. Experiments show that also in the multicellular stages the migration of the cells is controlled by propagating waves of cAMP and that the interaction between wave propagation and chemotaxis is sufficient to explain the principles of Dictyostelium morphogenesis. We are analysing the in-vivo spatio-temporal dynamics of the signaltransduction processes leading to polarised activation of the actin-myosin cytoskeleton. We make extensive use of quantitative imaging techniques to measure signal transduction dynamics during chemotactic cell movement of isolated cells as well as in individual cells in multicellular tissues ([6]; [7]; [8]). We monitor the organisation, dynamics and force generation of the cytoskeleton that results in movement using TIRF and traction force microscopy. We have developed continuous and discrete mathematical models to investigate the relation ship between signalling and cell movement to understand the dynamical interactions that govern the morphogenesis of this organism ([11]; [12]).

We are also interested in understanding how cell movement is controlled during the embryonic development of higher organisms, especially amniotes. Gastrulation is one of the key phases of the development of higher animals. It starts with the induction of the mesendoderm followed by movements of the epiblast to from the streak and ingression of the mesendoderm. It is not yet firmly established what controls the movement of the cells during this process. We investigate the role of chemotaxis in the control of gastrulation movements. During gastrulation the mesoderm and endoderm precursor cells move into the embryo to take up their correct topological positions. We have tracked the in-vivo migration of mesoderm cells, expressing fluorescent proteins, during gastrulation in the chick embryo and shown that their movement is controlled by a combined action of chemo-attractants and repellents belonging to the FGF, VEGF, PDGF and Wnt families ([1]; [9]; [13]; [14]). We have proposed that Fgf8 acts as a repellent for cells leaving the streak([13]). The mechanism through which this repulsion works has so far been

difficult to resolve experimentally. More recently Wnt 3, strongly expressed in the streak has been shown to act as a strong repellent for cardiac precursor cells, some of the first cells to ingress through the streak ([14]). Therefore it seems likely that Fgf8 and Wnt3 act in concert to guide cells away from the streak. Fgf4 acts as a potent attractant for mesoderm cells and since it is secreted by cells in the forming head-process it appears likely that this results in the migration of cells back towards the central midline. FgfR1 and FgfR3 receptors are expressed initially in the epiblast and subsequently in the migrating mesoderm. Migration of the cells out of the posterior streak appears to require the expression of VegfR2 and the cells migrate in response to VegfA expressed in the overlying epiblast. Inhibition of this receptor or depletion of its ligands results in complete inhibition of migration of the posterior streak cells (Yang, Chuai and Weijer, submitted). After migrating in the extra embryonic are these cells then aggregate to form blood islands that form the precursors of the vasculature. This process is controlled by expression of VegfA in the migrating cells, which is detected by VegfR2. We are now interested in trying to understand how cells detect these factors and translate this information to result in cell movement and how the signalling and movement are integrated to result in gastrulation.

The first sign of gastrulation is the formation of the primitive streak. The primitive streak, the site of invagination of the mesendoderm, forms at the posterior site of the embryo and extends in anterior direction until it covers about 80% of the epiblast. We have visualised the cell movement patterns occurring in the epithelial sheet of the epiblast during the formation of the primitive streak ([4]; [5]). Streak formation appears to involve to large scale counter rotating cell flows that merge at the site of streak formation. The flow patterns closely resemble a Stokes flow in a fluid in a bounded circular domain ([2]). Mechanisms underlying streak formation proposed so far involve oriented cell divisions driving elongation of the streak, cell-cell intercalation in the posterior streak, chemotaxis in response to a combination of repulsive and attractive signals and passive displacement of cells on a deformable matrix Our current hypothesis is that formation of the primitive streak also involves a combination of chemo-attractants and repellents ([2]; ([3]). We are currently testing this hypothesis both experimentally and through detailed computer simulations using a subcellular element model that is able to precisely model the rheological properties of cells and tissues ([10]).

References

[1] Markus Affolter and Cornelis J Weijer. Signaling to cytoskeletal dynamics during chemotaxis. *Dev Cell*, 9(1):19–34, Jul 2005.

[2] Manli Chuai and Cornelis J Weijer. The mechanisms underlying primitive streak formation in the chick embryo. *Curr Top Dev Biol*, 81:135–156, 2008.

[3] Manli Chuai and Cornelis J. Weijer. Who moves whom during primitive streak formation in the chick embryo. *HFSP Journal*, 3(2):71–76, 2009.

[4] Manli Chuai, Wei Zeng, Xuesong Yang, Veronika Boychenko, James A Glazier, and Cornelis J Weijer. Cell movement during chick primitive streak formation. *Dev Biol*, 296(1):137–149, Aug 2006.

[5] Cheng Cui, Xuesong Yang, Manli Chuai, James A Glazier, and Cornelis J Weijer. Analysis of tissue flow patterns during primitive streak formation in the chick embryo. *Dev Biol*, 284(1):37–47, Aug 2005.
[6] Dirk Dormann and Cornelis J Weijer. Imaging of cell migration. *EMBO J*, 25(15):3480–3493, Aug 2006.
[7] Dirk Dormann and Cornelis J Weijer. Visualizing signaling and cell movement during the multicellular stages of dictyostelium development. *Methods Mol Biol*, 346:297–309, 2006.
[8] Dirk Dormann, Gerti Weijer, Simon Dowler, and Cornelis J Weijer. In vivo analysis of 3-phosphoinositide dynamics during dictyostelium phagocytosis and chemotaxis. *J Cell Sci*, 117(Pt 26):6497–6509, Dec 2004.
[9] Tadahiro Iimura, Xuesong Yang, Cornelis J Weijer, and Olivier Pourqui. Dual mode of paraxial mesoderm formation during chick gastrulation. *Proc Natl Acad Sci U S A*, 104(8):2744–2749, Feb 2007.
[10] T. J. Newman. Modeling multicellular systems using subcellular elements. *Math. Biosci. Eng.*, 2(3):613–624 (electronic), 2005.
[11] Bakhtier Vasiev and Cornelis J. Weijer. Modelling *dictyostelium discoideum* morphogenesis. In *Mathematical models for biological pattern formation*, volume 121 of *IMA Vol. Math. Appl.*, pages 193–209. Springer, New York, 2001.
[12] Bakhtier Vasiev and Cornelis J. Weijer. Modelling of *dictyostelium discoideum* slug migration. *J. Theoret. Biol.*, 223(3):347–359, 2003.
[13] Xuesong Yang, Dirk Dormann, Andrea E Mnsterberg, and Cornelis J Weijer. Cell movement patterns during gastrulation in the chick are controlled by positive and negative chemotaxis mediated by fgf4 and fgf8. *Dev Cell*, 3(3):425–437, Sep 2002.
[14] Qiaoyun Yue, Laura Wagstaff, Xuesong Yang, Cornelis Weijer, and Andrea Munsterberg. Wnt3a-mediated chemorepulsion controls movement patterns of cardiac progenitors and requires RhoA function. *Development*, 135(6):1029–1037, 2008.

3D in vitro tissue models and bioelectronic life-cell monitoring for cell and tissue fingerprints: Basic data for mathematical modeling

Andrea Anneliese Robitzki

(joint work with Heinz-Georg Jahnke, Oliver Pänke)

Simulation of impedance spectra for 3D *in vitro* tissue models or spheres with different diameters and extracellular volume fractions 1. Impedimetric measurement and modeling of 3D *in vitro* tumour models Multicellular tumour spheroids that mimic a native cellular environment are widely used as model systems for testing of active pharmaceutical ingredients. To study effect of drugs on 3D spheres in real-time we designed and fabricated a novel type of 3D microcavity array for fast, non-destructive impedance spectroscopy and extracellular recording. Spheres are trapped between four gold electrodes. Fifteen individual 100 μm deep microcavities with sizes from 200 to 400 μm allow an optimal positioning during the measurement. Although the programmed cell death so-called apoptosis can be induced in mamma carcinoma and /or human melanoma spheres by camptothecin. Melanoma spheres do not show disintegration but displayed increased impedance magnitudes compared to untreated controls. The silicon-based electrode array can be used for the monitoring of any kind of 3D *in vitro* cell cultures. Since no adherence of cells or labelling is necessary the multifunctional sensor chip provides a basis for delivering basic data which can be used for mathematical modeling

and/or simulation of biophysical impedance spectra. A combination and correlation of laser scanning fluorescent microscopical images and bioelectronic fingerprints of each sphere model might improve the situation for modeling living cells and tissues [1, 2, 3].

Following the basic principle of data acquisition and processing each measurement starts with the recording of a reference spectrum with one pair of uncovered opposite electrodes. Then spectra for spheres covered electrodes are recorded. For data interpretation the most characteristic frequency (peak) can be determined. Subsequently the normalized impedance at this frequency is calculated as $\Delta Z = (|Z|covered - |Z|uncovered)/|Z|uncovered$. The most significant changes in electrode impedance occur in a range from 10 kHz to 1 MHz, when biological objects (3D spheres) are positioned between two electrodes [4].

The aim of e.g. an anticancer therapy is to inhibit tumour growth and tumour cell cycle progression and therefore, proliferation and initiation of apoptosis. Each of these desired effects of e.g. chemotherapeutics leads to a decrease of R_{ext}. R_{ext} depends on the conductivity of the interstitial, the size of the sphere and the volume fraction i. d. ratio of the volume of cells in relation to the volume of the 3D *in vitro* tissue model. A suppression of cellular proliferation leads to a stop of tissue growth which than shows lower absolute extra-cellular resistances R_{ext} than it is measured in larger, growing spheres. Induction of the programmed cell death i.d. apoptosis results in secondary necrosis indicated by the lysis of apoptotic bodies. Finally the volume fraction of such a 3D *in vitro* tissue decreases. The lower the volume fraction of the *in vitro* tissue the lower is R_{ext}. In this case the change of the conductivity of the interstitial caused by changes of the concentration and mobility of ions can be neglected [4, 5].

For visualization of changes in diameter and intracellular volume fraction of spheres, monitored by impedance spectra, these impedance spectra can be calculated for different equivalent circuit models. Equivalent circuit models of spheres are set up for the following cases (i) small volume (V), high intracellular volume fraction (F), (ii) large V, high F, (iii) small V, small F and (iv) small V, large F. The parameters for case (a) are fixed. Since small and large spheres show the same cross sectional area in a 3D biochip and its cavity or capillary, the models for large 3D *in vitro* tissue models are composed of a series connection of two models for small spheres. The smaller volume fraction can be modeled by smaller value for $R_{ext,sf}$ and $C_{mem,sf}$ and higher value for $R_{int,sf}$ compared with $R_{ext,hf}$, $C_{mem,hf}$, and Rint,hf. To clarify the problem, the values for $R_{ext,sf}$ and $R_{ext,hf}$ were chosen so, that where f is the frequency and Z_a, Z_c, Z_d are the total impedances of the circuit models described above.

At low frequencies the total impedances of the equivalent circuit models are similar to the total extracellular resistances and at high frequencies similar to the parallel connections of the total intracellular and the total extracellular resistances. Therefore, some models reflect similar impedances at low frequencies (below the β-dispersion) but different impedances at high frequencies (above the β-dispersion).

The impedances of models are different at low frequencies but similar at high frequencies.

2. An impedimetric microelectrode-based monitoring for label-free detection of tau hyperphosphorylation in human neuroblastoma cells For monitoring the modification of the Tau protein in Morbus Alzheimer brain slices and based on our findings and with regard to absence of neurofilament L alterations in okadaic acid treated neuroblasoma cells, we conclude that the observed impedimetric phenotype most likely reflects tau hyperphosphorylation induced pathological events. These aspects are tau accumulation and, potentially, early stages of cytotoxicity as well as tau aggregation. Effects of a potential Tau kinase inhibitor SRN-003-556 and okadaic acid mediating hyperphosporylation of Tau on seal resistance and membrane capacity could be documented. For calculating cell dependent parameters a simplified equivalent circuit model was used. The values for the parameters of CPE_{El} and R_{MEA} were obtained from measured $|Z|_{El}$and Phi_{El} of electrodes without cells and cell dependent parameters. R_{Seal} and C_{Mem} were obtained from measured $|Z|_{Cell}$ and Phi_{Cell} of electrodes with cells. Measured values of neuroblaszoma cells treated either with okadaic acid, SRN-003-556 alone, or both, SRN and okadaic acid for 10 h were analysed. Okadaic acid treated cell cultures gradually decreased the relative R_{Seal} with significant changes after 3, 5 and 10 h. When neuroblastoma cultures were pre-incubated with SRN-003-556 before okadaic acid was applied R_{Seal} values were not significantly changed after 3 h, slightly increased after 5 h and decreased after 10 h. In contrast, for okadaic acid treated cultures relative C_{Mem} values were increased after 5 and 10 h and whereas SRN-003-556 pre-incubated cultures only show an increase after 10 h [6].

References

[1] D. Kloss, M. Fischer, A. Rothermel, J. C. Simon, A. A. Robitzki, *Drug testing on 3D in vitro tissues trapped on a microcavity chip*, Lab Chip **8**,(2008), 879–884.

[2] D. Kloss, R. Kurz, H. -G. Jahnke, M. Fischer, A. Rothermel, U. Anderegg, J. C. Simon, A. A. Robitzki, *Microcavity array (MCA)-based biosensor chip for functional drug screening of 3D tissue models*, Biosens Bioelec. **23** (2008), 1473–1480.

[3] P. Wolf, A. Rothermel, A. G. Beck-Sickinger, A. A. Robitzki, *Microelectrode chip based real time monitoring of vital MCF-7 mamma carcinoma cells by impedance spectroscopy*, Biosens Bioelec. **24** (2008), 253–259.

[4] H. Thielecke, A. Mack, A. Robitzki, *Biohybrid screening systems: 3D in tissue biosensors for toxicity and therapeutical biomonitoring*, Fresenius J. Analyt. Chem., **369** (2001) 369, 23–29.

[5] H. Thielecke, A. Mack, A. A. Robitzki, *A tumor spheroid sensor for anticancer drug and gene therapy screening: 3D microtumors cultured in a microfluidic capillary system*, Biosensors & Bioelectronics **16** (2001), 261–269.

[6] H.-G. Jahnke, A. Rothermel, I. Sternberger, T.G. A. Mack, R. G. Kurz, O. Pnke O, F. Striggow, A. A. Robitzki, *An impedimetric microelectrode-based array sensor for label free detection of tau hyperphosphorylation in human cells*, Lab-On-Chip **9** (2009), 1422-1428.

Collective cell motility and self-organized sprout formation

András Czirók
(joint work with András Szabó)

Cell motility and its guidance through cell-cell contacts is a poorly understood, but fundamental process during vasculogenesis and several other morphogenic processes. Here we discuss two related problems: (i) how spontaneously polarized cells, i.e., cells that maintain their migratory direction in time, move in high density cultures [1], and (ii) how tissue cells can organize into expanding multicellular sprouts [2].

Self-organized flow patterns in monolayer cultures. Cell monolayers can exhibit self-organized flow patterns that are different both from a long-range ordered state where all cells move in similar directions, and from a disordered state where cells move diffusively and correlations decay rapidly both in space and time. Instead, an intriguing streaming behavior is observed. We distinguish two types of collective cell motility: endothelial cells behave more like a self-propelled liquid, characterized by quick separation of adjacent cells (mixing) and flows consisting of vortices and shear-lines separating domains moving in opposite directions. MDCK cells resemble an elastic solid, where cell-cell contacts are maintained longer, shear is diminished and an oscillatory movement is observed.

To better understand the emergence of collective flow patterns in cell monolayers, we studied a modified cellular Potts model (CPM), an often used way to deal with movements of close packed cells [3]. The main advantage of the CPM approach is that cell shape is explicitly represented, thus the simulation can resolve cell intercalation, an important mode of configuration rearrangement in high-density monolayers. To obtain a biologically plausible, yet simple model, we consider cell polarity (a self-propulsion direction persisting in time) and its determination by past cell movements in addition to the surface tension-like cell-cell adhesion and cell compressibility.

In the CPM lattice sites are labeled, and cells are represented as simple connected domains, i.e., a set of adjacent lattice sites sharing the same label σ, equal to the cell index i ($0 < i \leq N$). Cell movement is resulted by a series of elementary steps. Each step is an attempt to copy the label value from a random lattice site a to an adjacent site b. If the domains remain simply connected, thus cells do not break apart or form holes, the probability assignment rule ensures (i) the maintenance of a target cell size, (ii) adhesion of cells and (iii) active cell motion:

$$\ln p(a \to b) = \min[0, -\Delta H(a \to b) + w(a \to b)], \tag{1}$$

where w is a bias responsible for the dynamics and H is a goal function to be minimzed:

$$H = -\sum_{\langle x,x' \rangle} J(\sigma_x, \sigma_{x'}) + \lambda \sum_{k=1}^{N} \delta A_k^2. \tag{2}$$

The first term in Eq. (2) enumerates cell boundary lengths. The summation goes over adjacent lattice sites, and $J(i,j) = \alpha$, for $i,j > 0$, $i \neq j$ and zero otherwise. The second term in Eq. (2) is responsible to maintain a preferred cell area: for each cell k the deviation of its area from a pre-set value is denoted by δA_k.

Cellular self-propulsion was introduced through the cell polarity vector $\mathbf{p}_k$, which represent the preferred direction of movement [4], and set w according to

$$w(a \to b) = P \sum_{k=1}^{N} \frac{\mathbf{p}_k}{|\mathbf{p}_k|} \Delta \mathbf{x}_k(a \to b), \tag{3}$$

where P is a weight factor, and $\Delta \mathbf{x}_k$ is the displacement of the center of cell k, resulted by the elementary step considered. Motivated by statistical analysis of single cell motility data [5], polarity is determined as a memory of past cell displacements:

$$\mathbf{p}_k(t) = \sum_{\tau=0}^{\infty} h(\tau) \Delta \mathbf{x}_k(t-\tau), \tag{4}$$

where $h(\tau)$ is a memory kernel. Therefore, we assume a positive feedback loop involving cell movement and polarity.

Numerical simulations reveal that the propulsion term readily generates a self-propelled "fluid" or "solid" states with meandering streams containing several (10-20) cells [1]. The model can also exhibit a long-range ordered phase, when due to the boundary conditions all cells participate in a single, system-wide rotational movement. This state is reached by increasing either the compressibility, λ^{-1}, P or the duration of the memory h. By decreasing these parameters a completely disordered state is reached, when no streams are formed and there is no persistent motility. The main factor influencing the lateral size of the streams is λ.

Multicellular sprouts. During the formation of embryonic vasculature multicellular sprouts invade rapidly into avascular areas, eventually creating an interconnected network pattern. Sprout elongation, in turn, depends on a continuous supply of endothelial cells, streaming along the sprout towards its tip [6]. As long-term videomicroscopy of in vitro cell cultures reveal, many cell lines such as C6 gliomas, or 3T3 fibroblasts form multicellular linear arrangements in vitro, similar to the multicellular vasculogenic sprouts [2]. Close contact with elongated cells enhances and guides cell motility. Time-lapse microscopic records reveal that cells intensively move towards and within extending sprouts. After the sprouts became wider, cell motility diminishes again.

To explain these phenomena, we suggest that the surface of elongated cells are more attractive adhesion targets than the surfaces of well-spread, isotropic cells. The cell biological basis for such a preference is not yet known. We speculate that cells in elongated structures are under mechanical tension, and strained cells can have a stiffer cytoskeleton. Cells are able to respond to variations in extracellular matrix stiffness, and an analogous mechanotaxis utilizing cell-cell contacts is also feasible. For example, VE-cadherin, a major cell-cell adhesion receptor of vascular

endothelial cells, was recently shown to be incorporated in cell surface mechanosensing complexes.

To formulate and test the hypothesis that multicellular patterning is resulted by cell-guided motility, we modified the above described CPM. As we do not deal with a monolayer, we distinguish between cell free areas ($\sigma = 0$) and domains belonging to cells ($\sigma > 0$), i.e., $\chi = Supp(\sigma)$. The $J(i,j)$ interaction term, for $i \neq j$, is thus given as

$$J(i,j) = \begin{cases} \alpha, & \text{for } i,j > 0 \\ \beta, & \text{for } i = 0 \text{ or } j = 0. \end{cases} \tag{5}$$

The parameter β/α specifies the preference of cell-cell connections over cell-medium boundaries. For $\beta > \alpha$ or $\beta < \alpha$ cell-medium boundaries are preferred or penalized, respectively.

The bias $w(a \to b)$ represents a tendency to contact elongated cells:

$$w(a \to b) \sim [\chi(a) - \chi(b)] \sum_{\substack{c \\ \sigma_c \notin \{0, \sigma_a, \sigma_b\}}} \theta_{\sigma_c}. \tag{6}$$

The $\chi(a) - \chi(b)$ expression ensures that only cells (and not the medium) exhibit the preference. Furthermore, if site b is occupied by a cell ($\chi(b) = 1$) then no other cell ($\chi(a) = 1$) has an advantage to occupy that adhesion site. The summation in Eq. 6 goes over only those neighbor sites of b that belong to cells other than σ_a and σ_b. The measure of anisotropy for cell i is θ_i, obtained from the inertia tensor of the lattice domain representing the cell as $\theta_i = (\mu_i/\nu_i)^{1/2} - 1$, where $\mu_i \geq \nu_i$ are the two eigenvalues of the inertia tensor.

For certain parameter values the model indeed exhibits sprouting behavior, reminiscent of those observed in experiments. After the initial bud appears, the leading – elongated – cells attract other cells from the pool at the base of the sprout. Cells consisting the sprout continue to migrate until they connect to another cluster of cells. At that point the branch is established and becomes stable. Due to the effective surface tension present in the system, branches can also break up resulting in a coarsening effect. If sprouting takes place, then after an initial transient regime the balance of surface tension driven coarsening and the growth of new branches results in a quasi stationary state.

References

[1] A. Szabó, R. Ünnep, and A. Czirók. Collective cell flows in monolayer cultures. preprint.

[2] A. Szabo, E. Mehes, E. Kosa, and A. Czirok. Multicellular sprouting in vitro. *Biophys J*, 95(6):2702–2710, Sep 2008.

[3] J. A. Glazier and F. Graner. Simulation of the differential adhesion driven rearrangement of biological cells. *Phys Rev E Stat Phys Plasmas Fluids Relat Interdiscip Topics*, 47(3):2128–2154, Mar 1993.

[4] T.J. Newman. Modeling multicellular systems using subcellular elements. *Math. Biosci. Eng.*, 2:611–622, 2005.

[5] D. Selmeczi, S. Mosler, P. H. Hagedorn, N. B. Larsen, and H. Flyvbjerg. Cell motility as persistent random motion: theories from experiments. *Biophys J*, 89:912–31, 2005.

[6] E. D. Perryn, A. Czirok, and C. D. Little. Vascular sprout formation entails tissue deformations and ve-cadherin-dependent cell-autonomous motility. *Dev Biol*, 313:545–55, 2008.

Robustness of Pattern Formation in Development

Hans G. Othmer and David Umulis

In many developing organisms and tissues, the processes of pattern formation, growth and morphogenetic movements, are strongly buffered against perturbations such as changes in the ambient temperature or the loss of one copy of a gene, and the question is what mechanisms confer such resilience. We address this question in the specific context of scale-invariance: whether, and if so how, different size embryos lead to normally-proportioned adults. At one extreme is mosaic development in which removal of a part of a developing embryo at one stage results in the absence of that part, or parts that develop from it, in later stages. On the other hand, many systems show a high degree of regulation, particularly at early stages of development, and such regulation is usually described as robustness, in that the system can tolerate a certain class of perturbations.

To understand what we mean mathematically by robustness of a model, consider the dynamical system

$$\frac{dx}{dt} = F(x, p, S(t)) \qquad x(0) = x_0 \tag{1}$$

Three classes of 'perturbations' lead to three types of 'insensitivity' or 'robustness'. are as follows.

(1) Insensitivity with respect to inputs, by which we mean that *in the long run* the system ignores a certain class of inputs. This type of robustness is a characteristic of systems that adapt to constant signals, such as the signal transduction system in *E. coli*.

(2) Insensitivity with respect to changes in the vector field, *i.e., the function F in 1. This is captured in the notion of coarseness or structural stability: a vectorfield is structurally stable if its associated flow is orbit equivalent to the flow generated by any vectorfield in a sufficiently small neighborhood in a suitable topology. This is the broadest definition, for it includes changes in F itself, but it is a strictly local (in a suitable topology) result, except for linear vector fields.*

(3) *Insensitivity with respect to changes in parameters. Strictly speaking this is a subset of (2), but is often considered by itself.*

In this report we focus only on pattern formation, which involves the spatio-temporal control of gene expression by chemical substances called morphogens. A first step is to decide what characteristic of the dynamics is being tested for robustness, and in the context of spatial pattern formation, it is often a measure of the size of the system that is of interest with respect to robustness. Most development involves evolution from one pattern to another, and the antecedent of

the current stage provides what is called a prepattern for this stage. To understand how scaling enters in the simplest context, suppose that a single morphogen is produced at the boundary of a one-dimensional system, diffuses through the region, and decays via a first-order reaction. In dimensionless form the governing equations for the morphogen concentration c are

$$\frac{d^2c}{d\xi^2} = \lambda^2 c \qquad \text{for} \quad \xi \in (0,1)$$
$$-\frac{dc}{d\xi} = J \quad \text{at} \quad \xi = 0 \qquad\qquad \frac{dc}{d\xi} = 0 \quad \text{at} \quad \xi = 1,$$

where $\xi = x/L$, $\lambda^2 \equiv \kappa L^2/D$, $J = jL/D$, and κ, D, and j are the first-order decay rate, the diffusion coefficient, and the input flux, respectively. The solution is

$$c(\xi) = \frac{J}{\lambda}\left[\frac{e^{\lambda(2-\xi)} + e^{\lambda\xi}}{e^{2\lambda} - 1}\right] \equiv \frac{J}{\lambda}\,\phi(\xi) = \frac{j}{\sqrt{\kappa D}}\,\phi(\xi).$$

Thus the stationary distribution is characterized by the dimensionless parameter λ, which is the ratio of a diffusion time scale $\tau_D \equiv L^2/D$ and a kinetic time scale $\tau_K \equiv \kappa^{-1}$, and by a dimensional parameter that is the ratio of the input flux j to a characteristic velocity defined by the diffusion constant and the decay rate. The former determines how rapidly the morphogen concentration decays in space: the larger λ, the more rapidly the solution decays from its value at the source. If the input flux j is fixed, both the amplitude and the shape of the solution depend on L, and thus this simple mechanism is not robust under substantial variations in the length of a developing system.

To see how a patterning system based on reaction and diffusion can give rise to scale-invariant patterns, consider the following system. Let M denote the concentration of the morphogen and let C denote the concentration of a control species. Suppose that they react and diffuse in the region Ω according to the following equations.

$$\frac{\partial M}{\partial t} = \nabla \cdot (D(C)\nabla M) + \kappa(C)R(M) \quad \text{in} \quad \Omega$$
$$\frac{\partial C}{\partial t} = D_c\nabla^2 C + R \qquad\qquad\qquad\qquad \text{in} \quad \Omega$$

with homogeneous Neumann data on M and homogeneous Dirichlet data on C. As indicated, either or both of the diffusion coefficient and the characteristic kinetic time scale of the morphogen can be modulated by the control species [2]. In effect, the former changes the underlying space metric by changing the diffusion coefficient, and the latter changes the time scale by modulating the reaction rates. If only diffusion is modulated then the diffusion coefficients must scale as L^2, which in effect changes the metric, since the level sets of the control species provide a measure of distance from the boundary. If the kinetic scale factor κ is modulated then it must scale as L^{-2} to produce scale-invariant steady-state morphogen distributions. In the former case the time-scale for development is also

invariant, but in the latter it varies with L. The question is whether any known systems use some combination of these forms.

The common fruit fly *Drosophila melanogaster* has served as a model system for studies of genetics and pattern formation for the past century, and substantial progress in elucidating mechanisms of morphogen-mediated patterning has been made in recent years. Scale-invariance of morphogen patterning has been documented for two pathways: Anterior/Posterior (A/P) patterning of the embryonic axis by Bicoid protein [3, 4] and A/P patterning of wing imaginal discs by BMPs [6]. The range of lengths for which scale-invariance has been observed can be very large. For example, in Bicoid-mediated patterning, embryonic lengths between species of *Diptera* vary by five-fold [3], yet the spatial distribution of Bicoid scales appropriately. While the molecular mechanisms of embryonic and wing disc patterning are very distinct, the physics governing morphogen gradient formation are very similar at a coarse level. Both pathways are examples of source, diffusion, trapping (SDT) mechanisms and theoretical analysis demonstrates how a simple SDT mechanism can lead to scaling of the kinetics by L^{-2} [5]. Additional analysis of the SDT mechanism suggests that under certain conditions, changing the number of traps can also lead to invariance of the time-scale for development by modulation of the effective diffusion coefficient in proportion to L^2 [7]. According to analysis of the SDT model, scale-invariance can be automatically achieved if patterning occurs in a two-dimensional layer at the surface of the embryo, and if the total number of nuclei or binding sites is the same across species at similar stages. It has been shown experimentally that the condition on the number of nuclei holds [3].

Acknowledgements This research was supported in part by the US National Institutes of Health and the Minnesota Supercomputing Institute.

References

[1] L. Wolpert. Positional information and pattern formation. *Curr. Topics in Dev. Biol.*, 6:183–224, 1971.

[2] H. G. Othmer and E. F. Pate. Scale-invariance in reaction-diffusion models of spatial pattern formation. *Proc Natl Acad Sci U S A*, 77(7):4180–4184, July 1980.

[3] Thomas Gregor, William Bialek, Rob R de Ruyter van Steveninck, David W. Tank, and Eric F. Wieschaus. Diffusion and scaling during early embryonic pattern formation. *Proc Natl Acad Sci U S A*, 102(51):18403–18407, Dec 2005.

[4] Thomas Gregor,Eric F. Wieschaus, Alistair P. McGregor, William Bialek, and David W. Tank. Stability and nuclear dynamics of the bicoid morphogen gradient. *Cell*, 130:141-152, Jul 2007.

[5] D. Umulis, M.B. O'Connor, and H.G. Othmer. Robustness of embryonic spatial patterning in Drosophila melanogaster. *Curr. Top. Dev. Biol.*, 81:65–111, 2008.

[6] A. A. Teleman and S. M. Cohen. Dpp gradient formation in the Drosophila wing imaginal disc. *Cell*,103:971–980, 2000.

[7] D. M. Umulis. Analysis of dynamic morphogen scale-invariance. *J. Roy. Soc. Interface*, 2009. Available online at http://rsif.royalsocietypublishing.org/

A mesoscale shape energy for biomembranes

Matthias Röger
(joint work with Mark A. Peletier)

In this talk we discuss a mesoscale model for the self-assembling of amphiphilic molecules into thin bilayer structures. We propose an energy on a microscopic scale and pass to a mesoscale description on the level of densities of polar and nonpolar particles. To make a connection with well-known shape energies we pass with the mesoscale energy to a macroscopic limit.

1. Motivation. Phosphilipids are an example of amphiphilic molecules, having a polar head group and two hydrphobic tails. These lipids self-assemble – without forming chemical bonds – to remarkably stable bilayer structures that are the main building block of cell membranes.

Macroscopic models for the shape of such membranes or artificial vesicles consider these as closed, smooth, and boundaryless surfaces and prescribe an energy of the form

$$E(S) = \int_S k_1(H - H_0)^2 + k_2 K \, d\mathcal{H}^2. \tag{1}$$

Here $k_1 > 0$ and k_2, H_0 are constants, H and K are the (scalar) total and Gaussian curvature, and $\mathcal{H}^2$ is the two-dimensional Hausdorff measure. Whereas such models have been quite successful in describing the variety of vesicle shapes they cannot serve as an explanation of the self-assembling and the preference for uniformly thin and closed structures. Our goal is a mesoscopic model that demonstrates this preferences and that allows to compare the distinct contributions to the energy, induced by the resistance against stretching, fracture, and bending. We aim at a model that is as simple as possible but still keeps the essence of the amphiphilic behaviour.

2. Derivation of the mesoscopic energy. At a microscopic level we idealize lipid molecules as a tail bead and a head bead connected by a spring. We consider configurations of N lipid molecules given by the positions $X_i^t \in \mathbb{R}^3$ of tails and $X_i^h \in \mathbb{R}^3$ of heads, $i = 1, ..., N$. We then define an energy $E(\Psi)$ on distribution functions $\Psi(X)$, $X = \big((X_1^t, X_1^h), ..., (X_N^t, X_N^h)\big)$ that give the probability to observe a certain configuration. $E(\Psi)$ consists of a part that describes a spring energy for each single molecule and an interaction part that models the hydrophilic-hydrophobic repulsion:

$$E_{\text{micro}}(\Psi) = \sum_{i=1}^{N} \int h\big(|X_i^t - X_i^h|\big)\Psi(X)\, dX + E^{\text{int}}(\Psi),$$

where $h : \mathbb{R} \to \mathbb{R}$ describes the actual choice of spring energy.

To pass to a mesoscopic description we associate to a given distribution function Ψ *density functions* $\varrho_t(\Psi), \varrho_h(\Psi)$ of tail and head particles and derive an energy

for a given pair of density functions (r_t, r_h),

$$E_{\text{meso}}(r_t, r_h) \;=\; \inf\big\{E_{\text{micro}}(\Psi) \;:\; \varrho_t(\Psi) = r_t, \varrho_h(\Psi) = r_h\big\}. \tag{2}$$

One important simplifying assumption in our approach is that the interaction part of the microscopic energy only depends on the associated densities,

$$E^{\text{int}}(\Psi) \;=\; \int_{\mathbb{R}^3}\int_{\mathbb{R}^3} (1 - \varrho_t(\Psi)(x))\varrho_t(\Psi)(y)\kappa(|x-y|)\,dxdy,$$

where κ is a fixed interaction kernel and where by an incompressibility assumption $1 - \varrho_t(\Psi)$ represents the portion of polar (head or water) particles.

It turns out that the inf in (2) is in fact attained and that any minimizer is of the form $\Psi(X) = \Pi_{i=1}^N \psi(X_i^t, X_i^h)$ with a common distribution function ψ on $\mathbb{R}^3 \times \mathbb{R}^3$. The single molecule part of the microscale energy leads on the mesoscale to a contribution in form of a *Wasserstein distance* between the tail- and head densities. The energy depends on the total particle number N, which we consider to be large. We introduce $\varepsilon := N^{-\frac{1}{2}}$, choose a constant $M > 0$, and fix the total mass of tail and head particles to NM. We then consider the class of rescaled density functions of tail and head particles,

$$\tilde{K}_\varepsilon \;=\; \Big\{(u_\varepsilon, v_\varepsilon) \;:\; u_\varepsilon, v_\varepsilon : \mathbb{R}^n \to \mathbb{R},\, 0 \;\le\; u_\varepsilon + v_\varepsilon \;\le \varepsilon^{-1}, \int u_\varepsilon \;=\; \int v_\varepsilon \;=\; M.\Big\}$$

The mesoscale energy per particle is then for $(u_\varepsilon, v_\varepsilon) \in \tilde{K}_\varepsilon$ given by

$$\tilde{F}_\varepsilon(u_\varepsilon, v_\varepsilon) \;=\; d^{h,\varepsilon}\big(u_\varepsilon, v_\varepsilon\big) + \int_{\mathbb{R}^6} \Big(1 - \varepsilon u_\varepsilon(x)\Big)\varepsilon u_\varepsilon(y)\varepsilon^{-n+1}\kappa\Big(\frac{x-y}{\varepsilon}\Big)\,dxdy. \tag{3}$$

Here the first term on the right-hand side describes a Wasserstein-type distance term

$$d^{h,\varepsilon}\big(u_\varepsilon, v_\varepsilon\big) \;=\; \inf_{\psi}\Big\{\int_{\mathbb{R}^6} h\Big(\frac{|x-y|}{\varepsilon}\Big)\psi(x,y)\,dxdy\Big\},$$

where ψ is constrained to

$$u_\varepsilon(x) \;=\; \int \psi(x,y)\,dy, \quad v_\varepsilon(y) \;=\; \int \psi(x,y)\,dx.$$

3. Mathematical analysis. To understand the behaviour of the mesoscale energy and to allow for a rigorous mathematical analysis we do some further simplifications: We choose for the spring energy $h(r) = r$, restrict to two space dimensions $n = 2$, and replace the nonlocal repulsion energy, *i.e.* the second term in (3), by a local interfacial energy. This leads to a set of admissable density functions

$$K_\varepsilon \;=\; \Big\{(u_\varepsilon, v_\varepsilon) \;:\; u_\varepsilon, v_\varepsilon : \mathbb{R}^n \to \{0, \varepsilon^{-1}\},\, u_\varepsilon v_\varepsilon \;=\; 0,\, \int u_\varepsilon \;=\; \int v_\varepsilon \;=\; M\Big\}$$

and a mesoscale energy

$$F_\varepsilon(u_\varepsilon, v_\varepsilon) \;=\; \frac{1}{\varepsilon} d_1\big(u_\varepsilon, v_\varepsilon\big) + \varepsilon \int_{\mathbb{R}^2} |\nabla u_\varepsilon|, \tag{4}$$

where the first term is now the Monge–Kantorovich transport distance (Wasserstein-1 metric) and the last term describes the length of the boundary of the set $\{u_\varepsilon = \varepsilon^{-1}\}$.

In [1] we proved rigorously that this functional prefers structures that are uniformly thin (with an optimal thickness given by 2ε), that 'closed structures' are preferred, and that the bending of the structures is penalized. It is shown that a lower bound for the energy is given by $2M$. If we consider a sequence $(u_\varepsilon, v_\varepsilon)$ of structures whose energy is close to the optimal value $2M$ we can show that $u_\varepsilon, v_\varepsilon$ have to concentrate on a collection of curves $\gamma_i, i = 1, ..., Q$ as $\varepsilon \to 0$. Moreover, the energy F_ε is approximately of the following form:

$$(5) \qquad F_\varepsilon(u_\varepsilon, v_\varepsilon) \approx 2M + \sum_{i=1}^{Q} \mathcal{P}_{\text{stretching}}(\gamma_i) + \varepsilon \sum_{i=1}^{Q} \mathcal{P}_{\text{fracture}}(\gamma_i) + \frac{\varepsilon^2}{4} \sum_{i=1}^{Q} \int_{\gamma_i} \kappa_i^2,$$

where $\mathcal{P}_{\text{stretching}}$ penalizes a nonuniform thickness of the structures, $\mathcal{P}_{\text{fracture}}$ counts the number of open ends of the limit curves, and $\int_{\gamma_i} \kappa_i^2$ is the classical Euler bending energy for curves. This statement is made precise in form of a Gamma-convergence result for $\varepsilon^{-2}(F_\varepsilon - 2M)$ and a sharp lower bound estimate. For a precise statement and proofs of the results see [1]. The property that moderate-energy sequences have to concentrate on curves shows the self-assembling behaviour, whereas the penalization of stretching, fracture and bending is shown in the expansion (5) or the corresponding estimate in [1]. In particular, we observe that non-uniform thickness and fracture of the structures is indeed much more penalized than bending. Our result therefore justifies that uniform thickness and closedness enter the macroscale shape energies as hard constraints and that a bending energy emerges from the amphiphilic behaviour of the constituents of the membranes.

References

[1] M. A. Peletier and M. Röger, *Partial Localization, Lipid Bilayers, and the Elastica Functional*, Archive for Rational Mechanics and Analysis, **online first** (2008).

Mathematical models of stem cells renewal and differentiation

Anna Marciniak-Czochra

In higher organisms, a steady supply of somatic cells is accomplished by proliferation of various types of stem cells, which retained the capability for almost indefinite self-renewal. According to need, driven by hormonal signals from the organism, some stem cells commit to differentiation and maturation in the direction of more specialized cell lineages. A well-know example is provided by hematopoietic stem cells, which give rise to several lineages including precursors of erythrocytes (red cells), lymphocytes (white cells) and megakaryocytes (platelets), among other.

Hematopoiesis is a multi-step process, in which relatively small population of hematopoietic stem cells gives rise to all types of blood cells. This process is

based on asymmetric cell divisions leading to formation of more mature cells (differentiation process) and replenishment of the subpopulations of cells of different maturation stages (self-renewal). Understanding of the mechanisms governing hematopoiesis is of central interest in stem cell biology, especially because of its clinical impact. High regenerative properties of hematopoietic stem cells are used to reconstitute blood structure of patients after treatment with high-dose chemotherapy, which results in a rapid decline of blood cell counts. It is known that the dynamics of cell proliferation and differentiations is controlled by extracellular signaling molecules such as cytokines. However, the precise nature of this process is still unknown.

One established method of modeling of such hierarchical cell systems is to use a discrete collection of ordinary differential equations, each of which describes a well-defined differentiation stage. In such framework, a range of mathematical results have been obtained (such as stability and oscillation criteria), some of which are applicable to modeling of the underlying biological systems, e.g., [1].

Recently, we have proposed new multi-compartment models of hematopoiesis [3]. The models are motivated by the clinical data on blood reconstitution and on the experimental studies performed in the group of Prof. Anthony Ho and Dr. Wolfgang Wagner (Department of Inner Medicine V, University of Heidelberg). One of the crucial problems in the clinical practice is how to minimize the time needed for blood regeneration, i.e., how to accelerate this process. This issue is important, since during the period of blood reconstitution the immune system of patients is not working, which often leads to acute infections and death. Our work aims to approach the problem by investigation of the dynamics of hematopoiesis in dependence on the key parameters. In particular, the role of the asymmetry of cell division is investigated motivated by the recent experiments [2].

The models describe the dynamics of n cell subpopulations representing different differentiation stages and assuming different modes of regulation. At least six different compartments have been proposed although so far experimental data do not provide a precise distinction between these stages. The generic model has the form,

$$
\begin{aligned}
\frac{d}{dt}u_1 &= (2a_1(s)-1)p_1(s)u_1 - d_1u_1,\\
\frac{d}{dt}u_i &= (2a_i(s)-1)p_i(s)u_i + 2(1-a_{i-1}(s))p_{i-1}(s)u_{i-1} - d_iu_i,\\
\frac{d}{dt}u_n &= 2(1-a_{n-1}(s))p_{n-1}(s)u_{n-1} - d_nu_n,
\end{aligned}
\tag{1}
$$

where $i = 1, ..., n-1$. Parameters $a_i(s)$ describe fractions of self-renewal of the subpopulations (the fractions of the daughter cells, which do not differentiate) and parameters $p_i(s)$ denote the proliferation rates. Parameters d_i denote the decay rates for each subpopulation. s denotes a concentration of some signalling molecules (cytokines), which may regulate the differentiation and proliferation process. The level of the signal is assumed to be dependent on the level of mature

cells, and it is given by

$$s = \frac{1}{1 + ku_n}. \tag{2}$$

This dependence can be justified using a quasi-steady state approximation of the plausible dynamics of the cytokine molecules, [3]. The expression reflects the heuristic assumption that signal intensity achieves its maximum under absence of mature cells and decreases asymptotically to zero if level of mature cells increases.

Considering different plausible regulatory feedback mechanisms lead to different types of nonlinearities in the model equations. In particular, three different regulatory modes are considered: (1) $p_i(s) = \frac{p_i}{1+ku_n}$ and constant a_i, (2) constant p_i and $a_i(s) = \frac{a_i}{1+ku_n}$ and (3) $p_i(s) = \frac{p_i}{1+ku_n}$ and $a_i(s) = \frac{a_i}{1+ku_n}$.

Under some assumptions, the models have similar qualitative behavior, i.e., their solutions converge to a unique positive equilibrium. However, the models differ significantly concerning the rates of convergence, i.e., the time needed to approach a defined neighborhood of the steady state for given initial conditions. Regulation of proliferation rates, i.e., negative feedback between proliferation parameters and the value of the variable describing the number of mature cells, results in a prolonged increase of the model solutions. In contrast, analogous regulation of the ratio of self-renewal rate versus differentiation rate (regulation of the asymmetry of cell division) results in a faster increase of the solutions (faster convergence rate). In summary, the numerical simulations, performed for different initial conditions and different parameter sets, lead to the conclusion that the regulation of the asymmetry of cell divisions is significantly more efficient that the regulation of the proliferation rates.

The model (1) is based on the assumption that in each lineage of blood cell precursors, there exists a discrete chain of maturation stages, which are sequentially traversed. However, there are indications that the differentiation process is less rigid and that it involves transitions which are continuous, along with discrete ones. Assuming that the dynamics of differentiated precursors can be approximated by a continuous maturation model, we propose new mathematical models of stem cells renewal and differentiation. The model has the form of a system of a structured population equation coupled with ordinary differential equations. Let $w(t)$ denote a population of pluripotent hematopoietic stem cells, $v(t)$ population of mature cells and $u(x,\, t)$ - a population of committed cells and differentiated procursors, structured by the maturity level (denoted by x). Assuming that $x = x^*$ denotes the last maturity level of immature cells, and therefore, $u(x^*, t)$ describes the concentration of cells which differentiate into mature cells leads to the model

equations of the form,

$$\begin{aligned} \frac{d}{dt}w(t) &= \alpha(s)w(t), \\ \partial_t u(x,t) + \partial_x[g(x,s)u(x,t)] &= \beta(x,s)u(x,t), \\ g(0,s)u(0,t) &= g_w(s)w(t), \quad t>0, \\ \frac{d}{dt}v(t) &= g(x^*,s)u(x^*,t) - \mu v(t), \end{aligned} \tag{3}$$

with appropriate initial conditions. Here, $g(x,s) = 2[1-a(x,s)]p(x,s)$ describes the velocity of the maturation process with a signal function s depending on the concentration of mature cells v, given by a formula (2) (similarly as in multicompartment model). The parameters a_w and p_w satisfy the conditions, $a_w = a(0)$ and $p_w = p(0)$. Furthermore, $g_w(\cdot) = g(0,\cdot)$, $\alpha(s) = [2a_w(s)-1]p_w(s)$ and $\beta = p(x,s) - d(x)$.

Conditions of stability, which we obtained, seem to have interesting biological interpretations. The rate of HSC self-renewal (a_1) has to be larger than 1/2. In case of multi-compartment model this fraction has also to be larger than the corresponding rates for the other compartments. Otherwise, the compartment with the highest self-renewal potential takes over the stem cell function, whereas all up-stream compartments including the HSC compartment eventually become extinct. From that point of view stem cell behavior arises as a property of a whole population and not as a property of single cells. Interestingly, the structured model does not posses any semi-trivial steady states. If the structured subpopulation does not extinct, its level stays strictly positive. It shows that continuous differentiation may have different properties that the discrete one.

References

[1] C. Colijn and M.C. Mackey, *A mathematical model of hematopoiesis–I. Periodic chronic myelogenous leukemia*, J. Theor. Biol. **237** (2005), 117–32.

[2] A. Ho and W. Wagner, *The beauty of asymmetry: asymmetric divisions and self-renewal in the hematopoietic system*, Current Opinion in Hematologty, , **14** (2007), 330-336.

[3] A. Marciniak-Czochra, T. Stiehl, W. Jäger, A. Ho and W. Wagner, *Modeling asymmetric cell division in hematopietic stem cells regulation of self-renewal is essential for efficient repopulation*, Stem Cells and Development **17** (2008), 1–10.

Understanding Bacterial Operon Dynamics: Insight from Mathematical Modeling

Michael C. Mackey

(joint work with D. Horike, M. Santillán, N. Yildirim & E. S. Zeron)

This talk focussed on recent mathematical models for the dynamics in three paradigms of bacterial molecular biology:

(1) The *lac* (lactose) operon;
(2) The *trp* (tryptophan) operon; and
(3) The lysis/lysogeny switch in phage λ.

Using chemical kinetic models appropriate for examining dynamics in large populations of bacteria, we have studied a variety of phenomena observed experimentally. The examples chosen for discussion in this talk comprise three of the paradigmatic bacterial systems that have been studied by molecular biologists over the past fifty years, and because of the long history of attentions from experimentalists there is an abundance of available data relative to other molecular regulatory systems.

(1) The lactose operon (also known as the *lac* operon) is a molecular negative feedback control system in *E. coli* that allows the bacterium to utilize lactose as an alternative energy source in the absence of glucose. In the *lac* operon a three dimensional mathematical model seems to accurately capture the operon response to changes from a glucose to lactose medium [5]. This model is a reduction of a higher dimensional model originally presented in [2, 4]. Furthermore it is predicted [6, 7], and observed experimentally, that there should be bistable behaviour in the switch between the un-induced and induced states. However, there is still great controversy about the exact nature of this bistability [7]. Details of our work on this system and the most recent version of our models of the *lac* operon may be found in [7].

(2) The tryptophan operon (known also at the *trp* operon) is the control system in *E. coli* involved in the production of tryptophan. This control system involves several different types of negative feedback. The *trp* operon dynamics seem to be partially captured by a relatively simple system of nonlinear differential delay equations [1]. (The delays arise because of transcriptional and translational delays.) However, it is also clear that there are discrepancies between the existing (but rather sparse) temporal data on tryptophan and enzyme levels and the model predictions. We suspect that this is due to unknown biological mechanisms that have not been included in the modeling efforts.

    We further predict in a more recent and complete treatment [8] that there should be oscillations in tryptophan and enzyme concentrations under certain circumstances as has been reported experimentally.

(3) In the lysis/lysogeny switch of phage λ we have offered at least one explanation for the extraordinary stability of the lysogenous state [3]. This explanation, consistent with the experimental data, resolves a controversy that has been in existence for at least 20 years.

References

[1] M. Santillán & M.C. Mackey. "Dynamic regulation of the tryptophan operon: A modelling study and comparison with experimental data", Proc. Nat. Acad. Sci. (U.S.A.) (2001), **98**, 1364-1369.

[2] N. Yildirim & M.C. Mackey. "Feedback regulation in the lactose operon: A mathematical modeling study and comparison with experimental data", Biophy. J. (2003), **84**, 2841-2851.

[3] M. Santillán & M.C. Mackey. "Why the lysogenic state of phage λ is so stable: A mathematical modelling approach", Biophy. J. (2004) **86**, 75-84.

[4] M. Santillán & M.C. Mackey. "Influence of catabolite repression and inducer exclusion on the bistable behavior of the *lac* operon", Biophysical Journal (2004) **86**, 1282-1292.
[5] N. Yildirim, M. Santillán, D. Horike & M.C. Mackey. "Dynamics and bistability in a reduced model of the lactose operon", Chaos (2004) **14**, 279-292.
[6] M. Santillán, M.C. Mackey & E.S. Zeron. "Origin of bistability in the *lac* operon", Biophy. J. (2007), **92**, 3830-3842.
[7] M. Santillán & M. C. Mackey. "Quantitative approaches to the study of bistability in the *lac* operon of *Escherichia coli*", J. Roy. Soc. Interface (2008), **5**, S29-40.
[8] M. Santillán, E. S. Zeron & M. C. Mackey. "Systems biology of the tryptophan operon", Chapter 8 in **Mathematical Biology Research Trends** (ed. Lachlan B. Wilson), Nova Press (2008).

Modeling and analysis for the interaction of flow, chemical reactions, and mechanics in cell tissue

Maria Neuss-Radu
(joint work with Willi Jäger, Andro Mikelić)

1. Introduction

In this paper, we are studying model equations for processes in a porous elastic structure of cells. Experimental research on the physiology of living cells and tissues is providing more and more detailed information on the nano- and micro-scale. There is an urgent demand for mathematical modelling of reactive flow and transport and its interaction with elastic cell structures. Here we are formulating model equations on the fine scale, with ε as scale parameter, including

- Fluid flow in the extracellular space, diffusion, transport and reactions of substances in the fluid.
- Exchange of substances at the membranes.
- Diffusion of substances and chemical reactions inside the cells.
- Changes of the structures and their mechanical properties under the influence of chemical substances.

Using multiscale techniques, the scale limit is performed, and a macroscopic (effective) model system is derived preserving relevant information on the processes on the microscopic level. One obtains in the limit a system similar to the Biot-law in the theory of dynamic poroelasticity, however, due to the scaling resulting from the analysis of the real data, the macroscopic velocities are solving a differential equation containing only its spatial derivatives.

These investigations were motivated by questions asked by physiologists interested in perfusion and transport through tissue under varying mechanical and chemical conditions. The effective permeability of the tissue is changed under the influence of the mechanical changes caused in the solid phase. Experimental studies were performed by [2] for thin layers of endothelial cells. This cell layers were exposed either to chemicals or to shear stress caused by flow.

2. Setting of the microscopic model

Let $\varepsilon > 0$ be a sequence of strictly positive numbers tending to zero, and let $[0,T]$ denote a time interval, with $T > 0$. We consider the domain $\Omega = (0,1)^3$ consisting of two subdomains: the tissue part formed by the elastic cells and the fluid part representing the intercellular space. The tissue part is denoted by Ω^ε, the fluid part by Ω_f^ε, and the fluid-solid interface by $\Gamma^\varepsilon = \partial\Omega_f^\varepsilon \cap \partial\Omega^\varepsilon$. The boundary of the domain Ω consists of three parts $\partial\Omega = \Gamma_1 \cup \Gamma_2 \cup \Gamma_3$, where $\Gamma_1 = \{x_1 = 0\} \times (0,1)^2$, $\Gamma_2 = \{x_1 = 1\} \times (0,1)^2$ and $\Gamma_3 = \cup_{j=2,3}(\{x_j = 0\} \cup \{x_j = 1\}) \times (0,1)^2$. The outer unit normal to $\partial\Omega$ is denoted by ν. On the interface Γ^ε, we denote by ν the outer unit normal to the fluid part Ω_f^ε. The microscopic structure of Ω^ε and Ω_f^ε is periodic, and is obtained by the repetition of the scaled standard cell $Y = [0,1]^3$. We denote by Y_f and Y_s the fluid respectively the solid part of Y.

We start from the following dimensionless system on the microscopic scale, formulated in [1], describing the evolution of the common displacement function in the solid and fluid part u^ε, and of the concentrations of the two substances transported within the tissue $c_1^\varepsilon, c_2^\varepsilon$. This is a coupled system for the fluid/structure interaction:

$$\frac{\partial^2 u^\varepsilon}{\partial t^2} + \frac{1}{\varepsilon^2}\nabla p^\varepsilon = \Delta\left(\frac{\partial u^\varepsilon}{\partial t}\right) \qquad \text{in } \Omega_f^\varepsilon \times (0,T) \tag{1}$$

$$\nabla \cdot \left(\frac{\partial u^\varepsilon}{\partial t}\right) = 0 \qquad \text{in } \Omega_f^\varepsilon \times (0,T) \tag{2}$$

$$\frac{\partial^2 u^\varepsilon}{\partial t^2} = \frac{1}{\varepsilon^2}\nabla \cdot (A(\mathcal{F}(c_1^\varepsilon))D(u^\varepsilon)) \qquad \text{in } \Omega^\varepsilon \times (0,T) \tag{3}$$

$$u^\varepsilon \chi_{\Omega_f^\varepsilon} = u^\varepsilon \chi_{\Omega^\varepsilon} \qquad \text{on } \Gamma^\varepsilon \times (0,T) \tag{4}$$

$$\left(-\frac{1}{\varepsilon^2} p^\varepsilon I + 2D\left(\frac{\partial u^\varepsilon}{\partial t}\right)\right) \cdot \nu = \frac{1}{\varepsilon^2} AD(u^\varepsilon) \cdot \nu \qquad \text{on } \Gamma^\varepsilon \times (0,T) \tag{5}$$

with the elasticity coefficients changing as a function of cumulated quantity of c_1^ε:

$$\mathcal{F}(c_1^\varepsilon)(x,t) = (\mathcal{K} \star_t F(c_1^\varepsilon))(x,t) = \int_0^t \mathcal{K}(t-\tau) F(c_1^\varepsilon(x,\tau))\, d\tau,$$

and for the evolution of the concentrations:

$$\frac{\partial c_1^\varepsilon}{\partial t} - \nabla \cdot \left(D_1(c_2^\varepsilon)\nabla c_1^\varepsilon\right) = G_1 g_1(c_1^\varepsilon, c_2^\varepsilon) \qquad \text{in } \Omega^\varepsilon \times (0,T) \tag{6}$$

$$D_1(c_2^\varepsilon)\nabla c_1^\varepsilon \cdot \nu = 0 \qquad \text{on } \partial\Omega^\varepsilon \times (0,T) \tag{7}$$

$$c_1^\varepsilon(0) = c_{10} \qquad \text{in } \Omega^\varepsilon \tag{8}$$

$$\frac{\partial c_2^\varepsilon}{\partial t} + \frac{\partial u}{\partial t} \cdot \nabla c_2^\varepsilon - D_2 \Delta c_2^\varepsilon = G_2 g_2(c_2^\varepsilon) \qquad \text{in } \Omega_f^\varepsilon \times (0,T) \tag{9}$$

$$\frac{1}{K}\frac{\partial c_2^\varepsilon}{\partial t} - \frac{1}{K} D_2 \Delta c_2^\varepsilon = G_3 g_3(c_1^\varepsilon, c_2^\varepsilon) \qquad \text{in } \Omega^\varepsilon \times (0,T) \tag{10}$$

$$\left(\frac{\partial u}{\partial t} c_2^\varepsilon - D_2 \nabla c_2^\varepsilon\right) \chi_{\Omega_f^\varepsilon} \cdot \nu = -\frac{D_2}{K} \nabla c_2^\varepsilon \chi_{\Omega^\varepsilon} \cdot \nu \qquad \text{on } \Gamma^\varepsilon \times (0,T) \tag{11}$$

$$c_2^\varepsilon \chi_{\Omega_f^\varepsilon} = c_2^\varepsilon \chi_{\Omega^\varepsilon} \qquad \text{on } \Gamma^\varepsilon \times (0,T) \tag{12}$$

This system has to be closed by initial and boundary conditions at the outer boundary. Regarding the boundary conditions for u^ε, we impose zero normal stresses on Γ_1 in the fluid and solid, and given normal stresses $(\mathcal{S}_1, \mathcal{S}_2, \mathcal{S}_3)$ on Γ_2. On Γ_3 we suppose zero displacements. For the concentration c_1^ε, we have no-flux conditions on $\partial\Omega_s$. For c_2^ε, we impose Dirichlet boundary conditions on Γ_1, and no-flux conditions on the rest of $\partial\Omega$. For the precise formulation of the boundary and initial conditions, see [1] where also the existence, uniqueness and stability of a solution of problem (1)-(12), has been proven, under suitable assumptions on the data.

3. Effective equations

Based on uniform estimates on the microscopic solutions $(u^\varepsilon, c_1^\varepsilon, c_2^\varepsilon)$, we prove that they converge to the macroscopic quantities (u^0, c_1^0, c_2^0), satisfying the following effective equations.

- Homogenized system for the solid displacements

$$-Div_x \left\{ \int_{Y_s} A(\mathcal{F}(c_1^0))(D_x(u^0) + D_y(u^1))dy \right\} + |Y_f| \nabla_x p^0(t,x) = 0, \qquad \text{in } \Omega \times (0,T)$$

- Darcy's type equations for the averaged velocity. The two-scale approximation of the velocity is given by

$$v^0(t,x,y) = \partial_t u^0(t,x) + w^0(t,x,y) \cdot \chi_{Y_f}(y)$$

and satisfies

$$\int_{Y_f} v^0(t,x,y)dy - |Y_f| \partial_t u^0(t,x) = -K \nabla_x p^0(t,x), \qquad \text{in } \Omega \times (0,T)$$

$$div_x \int_{Y_f} v^0(t,x,y)dy = \int_{Y_s} div_y \left(\partial_t u^1\right)(t,x,y)dy, \qquad \text{in } \Omega \times (0,T)$$

with p^0 being the macroscopic approximation for the pressure.

- Homogenized system for the concentrations

$$|Y_s|\partial_t c_1^0 - div_x \left\{ \int_{Y_s} D_1(c_2^0)(\nabla_x c_1^0 + \nabla_y c_1^1) dy \right\} = |Y_s| g(c_1^0, c_2^0), \quad \text{in } \Omega \times (0,T)$$

$$\int_Y k(y) dy\, \partial_t c_2^0 - D_2 div_x \left\{ \int_Y k(y) \left(\nabla_x c_2^0 + \nabla_y c_2^1\right) dy \right\} +$$

$$+ div_x \left\{ \left(|Y_f| \partial_t u^0 + \int_{Y_f} \partial_t w^0 \right) c_2^0 \right\} = g_2(c_2^0)\chi_{\Omega_f} + g_3(c_1^0, c_2^0)\chi_{\Omega_s}, \quad \text{in } \Omega \times (0,T)$$

Here, the functions u^1, c_1^1, c_2^1 are periodic with respect to the microscopic variable y, and represent the first order terms in the asymptotic expansions of the functions $u^\varepsilon, c_1^\varepsilon$, and c_2^ε respectively. They are calculated from problems formulated on the standard cell.

References

[1] W. Jäger, A. Mikelić, M. Neuss-Radu: *Analysis of differential equations modelling the reactive flow through a deformable system of cells*, Arch. Rational Mech. Anal. **192** (2009), 331–374.

[2] J. Seebach, H. -J. Mädler, B. Wojciak-Stothard, H. -J. Schnittler: *Tyrosine phosphorylation and the small GTPase rac cross-talk in regulation of endothelial barrier function*, Thromb Haemost: Cell Signalling and Vessel Remodelling, **94** (2005), 620–629.

Axon growth in neural development: a multiscale problem

Giovanni Naldi

(joint work with Giacomo Aletti, Paola Causin)

In the embryo, undifferentiated sets of cells form organized patterns following pathways marked by chemical cues. At this small scale, cues are represented by single molecules, displaced from their release location by diffusion. Diffusion is the movement of matter from areas with higher concentrations (near the source) to areas of lower concentrations. Cells crawl along the positive gradient, towards the direction of increasing chemical signal, from the periphery to the source. This establishes the controlled flow of material needed to build structured tissues. Cells work out the right direction sensing the chemical cues released in the environment, filtering out noise. In this work we focus on the axon growth phenomena in neural development. To understand this mechanism, it is essential to dig into the process of gradient sensing. Cells try to detect very small differences in molecule concentration across their tiny diameter [3]. With this respect, they behave like an instrument that counts molecules in its surroundings and is allowed only a limited number of probings. The study of the measurement errors of such an instrument can explain the shape of the trajectories. In the developing nervous system,

axons find the targets they will innervate navigating through the extracellular environment. Pathfinding crucially relies on chemical cues and, among the others, guidance by gradients of diffusible ligands plays a key role (see, e.g., [4, 5, 6]). Detection and transduction of navigational cues is mediated by the growth cone (GC), a highly dynamic structure located at the axon tip. The cascade that leads to motility decisions is initiated by binding of the ligand with receptors located on the GC surface and on filopodia, thin filaments that protrude out from the distal part of the GC. In [1] a mathematical description of the growth cone transduction chain as a series of functional boxes characterized by input/output relations is provided. The model relies on the assumption that the characteristic time of independent concentration measures by growth cone receptors, the characteristic time of growth cone internal reorganization preceding motion and the characteristic time needed for a discernible axon turning belong to separated scales. The results give insight into the deterministic vs. stochastic regime of internal growth cone functions that are not readily accessible from experimental observations, pointing out a substantial equilibrium of the two contributions. The present Authors have extended the mathematical description of the growth cone transduction cascade of by adding a model of the gradient sensing process related to the theory of [2]. The study of the transmission of the noise-to-signal ratio allows to predict the variability of the gradient assay as a function of experimental parameters as the ligand concentration, both in the single and in the multiple ligand tests. As in [1], the model of axon chemotaxis we consider involves a synthetic mathematical representation of the transduction cascade of the GC. Different subsystems are identified, which lead from sensing of ligand concentration gradients to motion. Measures of concentration differences in the environment are produced by the Sensing Device Subsystem (SDSys). The Intracellular Transduction Subsystem (ITSys) processes the input from the SDSys producing a signal which, through the Motor Actuator Subsystem (MASys), causes the deviation of the GC trajectory. Intracellular transduction is a highly complex network. A gradient of chemoattractant (resp. chemorepellant) concentration orients the GC motion toward (resp. away from) the direction of the concentration source. Receptors located on the GC surface and filopodia bind to external ligands. The density function of bound receptors around the GC can be used to model the process of ligand concentration sensing. In the present model, we do not consider such a physical process, but we directly model the output of the SDBox as a mathematical object, the vector $\hat{\mathbf{P}}$ which triggers the deviation of the GC trajectory. The vector $\hat{\mathbf{P}}$ is a function of the gradient concentration: its direction is related to the orientation of the stimulus gradient, while its modulus is connected to the amplification produced by the GC transduction chain. According to a mechanical description, we ascribe the trajectory deviation to an equivalent force vector process $\mathbf{P}_t$ acting on an equivalent GC mass m. The process $\mathbf{P}_t$, output of the STBox is continuously attracted towards $\hat{\mathbf{P}}$. The role of the STBox is to compare the output $\hat{\mathbf{P}}$ of the SDBox, function of the external signals, against an "equivalent" actual force $\mathbf{P}_t$. In this process, a memory effect exists which damps the response. Moreover, we suppose that the

equivalent force $\mathbf{P}_t$ induces an acceleration only along the direction transversal to the trajectory. Consequently, if the axon moves with velocity vector $\mathbf{v}_g$ only the direction of the unit vector $\mathbf{e}_g$ is affected, leaving the velocity modulus constant. Based on the above considerations, the complete model of the GC motion reads: given $\hat{\mathbf{P}}$, find for $0 \leq t \leq T$ the GC position $\mathbf{x}_g = \mathbf{x}_g(t)$, such that

$$\dot{\mathbf{x}}_g = \mathbf{v}_g,\ \dot{\mathbf{v}}_g = \frac{\mathbf{P}_t \sin\beta}{m}\mathbf{e}^{\perp},\ d\mathbf{P}_t = -\frac{\mathbf{P}_t - \hat{\mathbf{P}}}{\tau}dt + \sigma\sqrt{\frac{2}{\tau}}d\mathbf{W}_t,$$
$$\mathbf{x}_g(0) = \mathbf{x}_g^0,\ \mathbf{v}_g(0) = v_g\mathbf{e}_g^0,\ \mathbf{P}_0 = \mathbf{P}^0,$$

where $\mathbf{W}_t$ denotes a two(three)dimensional Wiener process.

For the full 2D (or 3D) model we suppose the mesenchyme (extracellular matrix located within the embryonic mesoderm) to be a deformable elastic body that undergoes large deformations due to an imposed motion of its (computational) boundaries. In particular, we consider the mesenchyme to be an hyperelastic material. We adopt the simplest isotropic St. VenantKirchhoff model (the extracellular matrix is known to exhibit a viscoelastic mechanical behavior: a more detailed characterization of the mechanical properties should be done). For the numerical simulation we discretize the elastic problem with the finite element method, we obtain the field of matrix displacements and velocity $\mathbf{v}_\phi$. Moreover, we describe each axon as a $1D$ elastic fiber immersed in the extracellular matrix, modeled as a 2D continuum deformable body. The axon trajectory is represented by the successive positions of the axon head, given by $d\mathbf{x}_d/dt = \mathbf{v}_g(t) + \mathbf{v}_\phi$: an intrinsic growth velocity plus the time rate variation of the matrix shape. The variation of $\mathbf{v}_g(t)$ is given by $d\mathbf{v}_g(t) = \mathbf{v}_g^{(1)} + \mathbf{v}_g^{(2)}$, where the first component is due to matrix deformation while the second term is related to chemical cues (microscopic model of filopodia), axon mechanical properties (bending vs. axial stiffness), and stochastic noise. Diffusible substances released in the extracellular matrix by target regions are modeled by diffusionreaction system. The process is supposed to be quasi-stationary due to the fact that the concentration field reaches an equilibrium faster than the characteristic time of axon outgrowth (at each time, the geometry of the extracellular matrix domain is given by the solution of the continuum mechanics problem). In Figure 1 we show an example of a numerical simulation for the whole process. We integrate numerically the SDE complete model by considering 500 axons, randomly seeded along the bottom boundary and assigned different birth times, a prescribed motion is imposed to the top and bottom borders. A weak attractive diffusible cue is placed in the top-central part of the domain while repulsive cues are placed close to the corners. A $3D$ model is being developed in order to obtain a more realistic representation of in vivo phenomena: the analysis of such a model with numerical results and comparisons with respect the biological data will be appear in a forthcoming paper.

References

[1] G. Aletti, P. Causin, *Mathematical characterisation of the transduction chain in growth cone pathfinding*, IET systems biology, **2** (2008), 150–161.

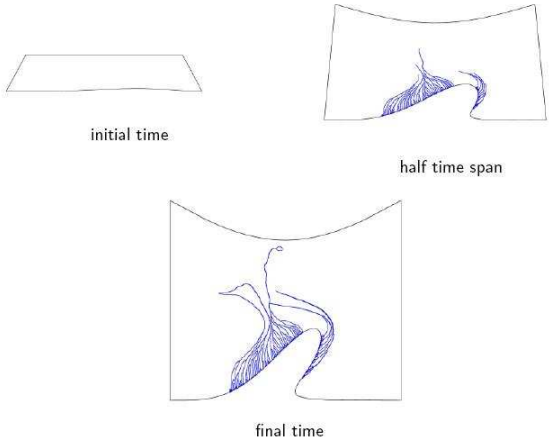

FIGURE 1. A numerical result for the complete model.

[2] G. Aletti, P. Causin, G. Naldi, *Mathematical characterisation of the transduction chain in growth cone pathfinding*, IET systems biology, **2** (2008), 150–161.
[3] H. Berg, E. Purcell, *Physics of chemoreception*, Biophys. J. **20** (1977), 193–219.
[4] B. Mueller, *Growth cone guidance: first steps towards a deeper understanding*, Annu. Rev. Neurosci. **22** (1999), 351–601.
[5] H. Song, M. M. Poo, *The cell biology of neuronal navigation*, Nat. Cell Biol. **3** (2001), E81E88.
[6] M. Tessier-Lavigne, C. Goodman, *The molecular biology of axon guidance*, Science **274** (1996), 1123–1133.

The mechanics of cell migration: inverse and direct problem

DAVIDE AMBROSI

Cell locomotion occurs through complex interactions that involve, among others, actin polymerization, matrix degradation, chemical signaling, adhesion and pulling on substrate and fibers. When focusing on mechanical aspects only, a major issue is the determination of the dynamic action of the cells on the environment during migration: the cells adhere, pull on the surrounding matrix and move forward.
Continuum mechanics seems to be the correct mathematical framework to address a quantitative understanding of the force balance that occur at the surface that separates the cell and the deformable environment. However, there are two main reasons that make this insight not trivial.
The first motivation is that the involved spatial scales are small and direct measurement of the forces is a non–trivial task. In some cases these data are experimentally obtained, but in configurations that are quite far from the physiological environment. The second and even more challenging difficulty is that cells are a non–standard mechanical system at all; they are made by several components of very different mechanical behaviour and, even more importantly, the main mechanical component of the cell (the citoskeleton) is formed by a polimeric network that continously polimerizes and de-polimerizes at the extremities, thus generating the *active* self–deformation of the cell that determines its ability to migrate.

In the talk given at the MFO it has been shown that cell traction can be fruitfully studied as an *inverse* problem. A quantitative methodology in this respect has been proposed in 1996 by Dembo *et al.* [3], an approach further improved by Dembo and Wang in 1999 [4]. They deduce the traction exerted by a fibroblast on a polyacrylamide substrate from the measured displacement of several fluorescent beads merged in the upper layer of the gel.

Under assumptions of isotropy and homogeneity, the deformations are supposed to be small and the equations of linearized elasticity apply. Although the displacement of the substrate $\mathbf{u}(\mathbf{x})$ is known at some points on the surface, say $\mathbf{u}_o$ its value, we cannot plug this directly into the elasticity operator to obtain $\mathbf{f}$. The motivations are twofold: since $\mathbf{u}_o$ is known in some portions of the domain only, there are many $\mathbf{f}$ that can produce this known displacement. Secondly, inverse problems are well known to excite high frequency components of the (always present) experimental error and a regularization procedure is therefore needed.
Following Dembo and Wang, the solution $\mathbf{u}$ of the elasticity equation is written in integral form using the Green tensor $\mathbf{G}$ of the elasticity equation for the half space domain (Boussinesq problem). The force per unit surface generating a displacement near to the experimental one (in a suitable sense) is obtained by discrete minimiaztion of the quadratic mean error under force penalization to ensure regularization (Tikhonov method).

The same issue studied illustrated above can be alternatively addressed using classical functional analysis. The minimization of the distance between the measured and the computed displacement under penalization of the force magnitude is stated *before* the elasticity equations are solved. Standard derivation of the cost function leads to two sets of elastic–type problems: the direct and the adjoint one.

The three–dimensional elasticity system of equations is approximated by a two–dimensional plane–stress one by vertical averaging along an *effective thickness* h:

$$-\hat{\mu}\Delta\mathbf{u} - (\hat{\mu}+\hat{\lambda})\nabla(\nabla\cdot\mathbf{u}) = \mathbf{f}, \qquad \mathbf{u}|_{\partial\Omega} = 0, \tag{1}$$

where

$$\hat{\mu} = h\frac{E}{2(1+\nu)}, \qquad \hat{\lambda} = h\frac{E\nu}{1-\nu^2}.$$

and E and ν are the Young modulus and the Poisson ratio respectively. h is the averaging depth fixed by the depth of field of the microscope. In our case h is 1.5 microns; the beads lying below such vertical coordinate are not in focus and therefore their position is not measured. Consequently the displacement $\mathbf{u}$ should be understood as the average displacement along h, which is nearly the displacement of the center of the beads.
The functional $J(\mathbf{f})$ measures the difference between the displacement field produced by $\mathbf{f}$ and the experimental one $\mathbf{u}_0$ under penalization of the square norm of the force field itself. It is defined as follows:

$$J(\mathbf{f}) = \int_{\Omega_0} |\mathbf{u}-\mathbf{u}_0|^2\, dV + \varepsilon \int_{\Omega} |\mathbf{f}|^2 dV, \tag{2}$$

where ε is a real positive number. We look for $\mathbf{g}$ minimizing J:

$$J(\mathbf{g}) \leq J(\mathbf{f}), \qquad \forall \mathbf{f} \in V_c, \tag{3}$$

where $V_c \subset L^2(\Omega)$ is the space of the finite energy functions with support in Ω_c. Variational derivation of $J(\mathbf{f})$ and introduction of the adjoint differential equation yields the following direct and inverse systems of partial differential equations [1]

$$\begin{aligned} -\hat{\mu}\Delta\mathbf{u} - (\hat{\mu}+\hat{\lambda})\nabla(\nabla\cdot\mathbf{u}) &= -\frac{\chi_c}{\varepsilon}\mathbf{p}, \qquad \mathbf{u}|_{\partial\Omega} = 0, \\ -\hat{\mu}\Delta\mathbf{p} - (\hat{\mu}+\hat{\lambda})\nabla(\nabla\cdot\mathbf{p}) &= \chi_o\mathbf{u} - \mathbf{u}_0, \qquad \mathbf{p}|_{\partial\Omega} = 0. \end{aligned} \tag{4}$$

The value of the penalty parameter ε and the averaging depth h can be fixed on the basis of arguments suggested by modal analysis or by the L-curve criterion. The unknown of the adjoint equation is just the shear stress exerted by the cells we are looking for. The two systems of equations can then be solved numerically by a coupled finite element discretization.

In the Oberwolfach meeting the discussion has focused on the regularity properties that characterize the solution of equations (4) depending on the smoothness of the datum $\mathbf{u}_0$. Moreover it has been shown as the above methodology can be applied to 3D cell migration too, a much more complicated framework where inhomogeneity and anisotropy prevent the use of other methods. Assuming that collagen fibers play no mechanical role, in the linearized case the following direct and inverse problem can be formally deduced:

$$\begin{aligned} &\nabla\cdot\mathbf{T}(\nabla\mathbf{u}) = 0 \qquad \mathbf{T}(\nabla\mathbf{u})\mathbf{n} = -\frac{1}{\varepsilon}(\mathbf{p}-\bar{\mathbf{p}}) \text{ on } \partial\Omega_c \qquad \mathbf{u} = 0 \text{ on } \partial\Omega \\ &\nabla\cdot\mathbf{T}(\nabla\mathbf{p}) = \chi_o\mathbf{u} - \mathbf{u}_o \qquad \mathbf{T}(\nabla\mathbf{p})\mathbf{n} = 0 \text{ on } \partial\Omega_c \qquad \mathbf{p} = 0 \text{ on } \partial\Omega \end{aligned}$$

where $\mathbf{T}$ is the Cauchy stress tensor, $\bar{\mathbf{p}}$ is the surface average value of $\mathbf{p}$ on $\partial\Omega_c$ and $\mathbf{n}$ is the tensor normal to $\partial\Omega_c$. In the nonlinear case the equations should be conveniently re-stated in a material system of coordinates, the adjoint operator depends on $\mathbf{u}$ and the second equation takes a more complicated form. If fibers have a mechanical role, it will be $\mathbf{T}(\nabla\mathbf{u}, \mathbf{m})$ where $\mathbf{m}(\mathbf{x})$ is the density of fibers directed as $\mathbf{m}$ in $\mathbf{x}$. The details of this generalization remain to explored.

References

[1] D. Ambrosi, Cellular traction as an inverse problem, *SIAM J. Appl. Math*, 66:2049–2060 (2006).

[2] D. Ambrosi, A. Duperray, V. Peschetola and C. Verdier, *Traction patterns of tumor cells*, J. Math. Biol., 58:163-181 (2009).

[3] Dembo, M., Oliver, T., Ishihara, A. and Jacobson, K., Imaging the traction stresses exerted by locomoting cells with elastic substratum method, *Biophys. J.*, **70**:2008–2022 (1996).

[4] Dembo, M. and Wang, Y. L., Stresses at the cell-to-substrate interface during locomotion of fibroblasts, *Biophys. J.*, 76:2307-2316 (1999).

Stability Analysis of a Simplified Yet Complete Model for Chronic Myelegeneous Leukemia

Marie Doumic Jauffret
(joint work with Peter Kim and Benoît Perthame)

We analyze the asymptotic behavior of a partial differential equation (PDE) model for hematopoiesis. This PDE model is derived from the original agent-based model formulated by Roeder *et al.* in [1], and it describes the progression of blood cell development from the stem cell to the terminally differentiated state.

To conduct our analysis, we depart from the PDE model proposed by Kim et al in [2], which proved to coincide very well with the simulation results obtained by Roeder *et al.* We further simplify the PDE model to make it amenable to analysis and justify the validity of our approximations using numerical simulations. An analysis of the simplified PDE model proves to exhibit very similar properties than the original agent-based model, even if for slightly different coefficients. Hence, the simplified model is of value in understanding the dynamics of hematopoiesis and of chronic myelogeneous leukemia, and it presents the advantage of having fewer parameters, which makes comparison with both experimental data and alternative models much easier.

Chronic myelogenous leukemia (CML) is a cancer of the blood and bone marrow that results in the uncontrolled growth of myeloid blood cells. More than 90% of all CML cases are associated with a gene abnormality, known as the Philadelphia (Ph) chromosome. In addition, CML is highly responsive to treatment by the drug imatinib that specifically targets the gene abnormality.

Recently, CML has been the focus of several mathematical models. A new paradigm of cancer development emerged from the idea of cancer stem cells (Bonnet et al, 1997). This hypothesis states that a variety of cancers originate from a self-replenishing, cancer population, now known as cancer stem cells. Using this idea, Roeder *et al.* developed a mathematical model of CML stem cells. In their model, leukemia stem cells continually circulate between proliferating and quiescent states.

We take the PDE model in [2] and simplify it as much as possible without altering the fundamental assumptions of Roeder *et al.*. It leads to three possible approximations, the simplest one being given by the following model:

$$\frac{dA}{dt} = -\omega(\overline{\Omega})A(t) + \int_0^1 \alpha(x,A)\Omega(x,t)dx, \qquad 0 \le x \le 1, \quad t \ge 0, \tag{1}$$

$$\frac{\partial \Omega^*}{\partial t} + \rho_d \frac{\partial \Omega^*}{\partial x} = \left(-\alpha(x,A) + b\right)\Omega(x,t) \tag{2}$$

with boundary condition

$$\Omega(0,t) = \frac{\omega(\overline{\Omega})}{\rho_d}A(t), \qquad \overline{\Omega}(t) = \int_0^1 \Omega(x,t)dx. \tag{3}$$

In this system, Ω represents the density of proliferating and maturing stem cells, whereas A is the density of fully immature quiescent cells. Mature cells are given

by $\Omega(t, x = 1)$. Cells can exchange compartments with rates $\alpha(x, A)$ and $\omega(\overline{\Omega})$, where $\overline{\Omega} = \int_0^1 \Omega(t, x)dx$ is the total population of proliferating cells. Both α and ω are decreasing functions of the population - in order to model competition for room in each of the compartment. The average renewal term is given by b, and the maturing speed by ρ_d.

The originality of this model is to take into account reversible maturity: when they become quiescent, cells replenish themselves and become immature again.

To conduct the analysis we use duality arguments related to the "General Relative Entropy" method introduced by B. Perthame, L. Rhyzik, P. Michel, S. Mischler (see [3]). This method requires us to handle the eigenvalue problem and its adjoint, which we do first, and then use them to build entropy functionals. Another method is to reduce the system to a delay differential equation (DDE), and we also comment on how this is possible.

The main mathematical results are given by the following proposition.

Proposition.

Let $\alpha(x, \cdot)$ be continuous positive decreasing function for all x and $\omega(\cdot)$ bounded. Let us denote

$$P(A) = \int_0^1 \alpha(x, A) e^{\int_0^x \frac{b-\alpha(y,A)}{\rho_d} dy} dx.$$

- *Zero is always a steady state, and there is a nonzero steady state (which is unique)* iff $P(0) > \rho_d$.
- *If for A large enough $P(A) < \rho_d$, then any solution $\big(\Omega(t, x), A(t)\big)$ of (1)–(3) remains bounded for all $t \geq 0$, i.e., $A \in L^\infty(0, \infty)$ and $\Omega \in L^\infty((0, \infty) \times (0, 1))$.*
- *If $P(0) \leq \rho_d$, then the zero steady state is globally attractive. If on the contrary $P(0) > \rho_d$, then the zero steady state is unstable.*

References

[1] I. Roeder, M. Horn, I. Glauche, A. Hochhaus, M.C. Mueller, M. Loeffler, M, *Dynamic modeling of imatinib-treated chronic myeloid leukemia: functional insights and clinical implications*, Nature Medicine **12 (10)** (2006), 1181–1184.

[2] P.S. Kim, P.P. Lee, D. Levy,*Modeling imatinib-treated chronic myelogenous leukemia: reducing the complexity of agent-based models*, Bulletin of Mathematical Biology **70 (3)** (2007), 728–44.

[3] B. Perthame, *Transport Equations in Biology*, Birkhauser (2007).

Intracellular Noise and Quorum Sensing

Johannes, Müller

(joint work with Alexandra Hutzenthaler, Robert Schlicht)

One of the challenges in mathematical biology is to cope with better and better measurements, that meanwhile deal with smallest entities like single cells, or even

single molecules. Models are forced to acknowledge – at least up to a certain degree – discreteness and the stochasticity of the subject under investigation. Following the approach [2, 4], in [3] a model for stochasticity in gene expression is described and analyzed. In that model, it is assumed that the gene product (mRNA or a protein) is present in large numbers, while the gene itself only exists in one copy. Transcription is regulated by the interaction of regulatory protein and a promotor region: binding of the regulatory protein to the promotor region alters the transcription rate. It is possible to treat the gene product as a continuous variable, while the state of the gene (bound or unbound to the regulatory protein) is a binary random variable. This approach yields a correlated random walk for the density of gene products.

In [3] especially a positive feedback loop (the gene product and the regulatory protein are identical, and the transcription rate is much higher if the protein is bound to the promotor) is considered. The considerations show that the distribution describing the amount of the gene product is (in general) bimodal. The two maxima correspond to the bistability of the corresponding deterministic model.

This outcome allows us to simplify the description of a cell by assuming an activated and a resting state. The intracellular noise allows a single cell to switch back and forth between these two states. In case of Quorum Sensing – an intercellular communication system – the gene product is able to freely pass the cell membrane. In contrast to other situations, where cells act independently with respect to the gene products under consideration, in Quorum Sensing there is a common pool for the gene product. Let us denote by x the amount of this gene product. Given x, the rate for a cell to jump from resting to activated state is $\nu(x)$, while that for deactivation is $\mu(x)$. Let us assume that we have N cells. The state of the system is given by a point (x, n) in the product space $\mathbf{R}_+ \times \{0, .., N\}$, where the first component indicates the amount of gene product, the second component the number of activated cells. If we condition on the number of activated cells n, the gene product follows a deterministic law

$$\dot{x} = \alpha N + \beta n - \gamma x =: v_n(x)$$

where α is the basic, and $\alpha + \beta$ the increased production rate of the gene product, while γ denotes the degradation rate. Furthermore, let (for fixed x) $L(x) \in \mathbf{R}^{(N+1)\times(N+1)}$ denote the infinitesimal generator of the random walk on $\{0, .., N\}$ given by the stochastic process for the number of activated cells n. That is, $(L(x))_{(i,n)}$ is the infinitesimal transition probability from i to n activated cells. Let $\pi(n; x)$ be the invariant distribution for given x.

If we denote the probability density of the state (x, n) at time t by $p(t, x, n)$, the complete model then has the following form (see e.g. [1, 3]),

$$\partial_t p(t, x, n) + \partial_x (v_n(x) p(t, x, n)) = \sum_{i=0}^{N} (L(x))_{(i,n)} p(t, x, i).$$

Defining the mean velocity $\overline{v}(x) = \sum_{i=0}^{N} v_n(x)\pi(n;x)$, and introducing – slightly artificially – the small variable ε, we obtain

$$\varepsilon^2\partial_t p(t,x,n) + \varepsilon^2\partial_x(\overline{v}(x)p(t,x,n)) + \varepsilon\partial_x([v_n(x) - \overline{v}(x)]p(t,x,n)) = \sum_{i=0}^{N}(L(x))_{(i,n)}p(t,x,i).$$

This is, the original model coincides with the model given in this equation only for $\varepsilon = 1$. However, taking the limit $\varepsilon \to 0$, we obtain (following the procedure described in [1]) an approximation of the density by $p(t,x,n) \approx \pi(n;x)\ h(t,x)$, where the marginal distribution $h(t,x)$ obeys the equation

$$\partial_t h(t,x) \quad = \quad -\partial_x\left(g(x)h(t,x)\right) + \partial_x\left(a(x)\partial_x h(t,x)\right)$$

with zero flux boundary conditions at $x_0 = \alpha N/\gamma$ and $x_1 = (\alpha+\beta)N/\gamma$. The functions $g(x)$ and $a(x)$ are defined via

$$g(x) = \alpha N - \gamma x + \frac{\beta N\nu(x)}{\mu(x)+\nu(x)} + \frac{\beta^2 N(\nu(x)\partial_x\mu(x) - \mu(x)\partial_x\nu(x))}{(\mu(x)+\nu(x))^4)}\ (\nu(x)-\mu(x))$$

and

$$a(x) = \frac{\beta^2 N\nu(x)\mu(x)}{(\mu(x)+\nu(x))^3}.$$

Numerical simulations show that this reduced model approximates quite well the marginal distribution for x for the original model.

We now relate the variables to a given volume V, i.e. we introduce cell densities ($\rho = N/V$) and, correspondingly, signal substance density ($z = x/V$). The rates $\mu(.)$ and $\nu(.)$ then depend on the density of signaling molecules, i.e. they are functions of z rather than x. We define the average net production rate of signaling substance $f(z)$ and a second function $g_1(z)$ (that does not play a role for $V \to \infty$)

$$\begin{aligned} f(z) \quad &= \quad \alpha\rho + \frac{\beta\rho\nu(z)}{\mu(z)+\nu(z)} - \gamma z, \\ g_1(z) \quad &= \quad \frac{\beta^2\rho(\nu(z)\partial_z\mu(z) - \mu(z)\partial_z\nu(z))}{(\mu(z)+\nu(z))^4)}\ (\nu(z)-\mu(z)). \end{aligned}$$

We find for the rescaled equations

$$\partial_t h(t,z) = -\partial_z\left((f(z) + g_1(z)/V)h(t,z)\right) + \frac{1}{V}\partial_z\left(a_1(z)\partial_z h(t,z)\right),$$

with

$$a_1(z) = \frac{\beta^2\rho\nu(z)\mu(z)}{(\mu(z)+\nu(z))^3}.$$

We are now interested in stationary states for medium and large populations, i.e. for the limits $V \to \infty$ and $t \to \infty$. The result depends on the order in which the limits are taken.

(1) First $V \to \infty$:

We obtain a hyperbolic PDE, which can be solved via the characteristics,

$$\dot{z} = f(z).$$

This is the deterministic model for this biological system. The solution of the ODE tends to the roots of $f(z)$, and the stability can be determined by inspecting the derivative of f at these points. The system exhibits bistability and hysteresis.

(2) First $t \to \infty$:
We obtain the stationary solutions of the PDE for $h(z,t)$,

$$0 = -\partial_z \left((f(z) + g_1(z)/V)h(z) \right) + \frac{1}{V} \partial_z \left(a_1(z) \partial_z h(z) \right).$$

which reads

$$h(z;V) = c(V;z_0) \left(e^{\int_{z_0}^{z} f(\zeta)/a_1(\zeta)\, d\zeta} \right)^V \left(e^{\int_{z_0}^{z} g_1(\zeta)/a_1(\zeta)\, d\zeta} \right).$$

The constant $c(V;z_0)$ is used to normalize the L_1 norm of $h(z)$ to one. For $V \to \infty$, the function $h(z;V)$ tends to a point mass centered at the (generically unique) maximum of $h(z;V)$, i.e. on roots of $f(z)$, which correspond to locally stable stationary states in the ODE $\dot{z} = f(z)$. Hence, as expected, we again find the stationary states of the deterministic model. It is unexpected, though, that the bistability and hysteresis is lost.

Summary: Stochasticity may destroy hysteresis for slowly changing parameters. Our finding can be interpreted as the possibility of the system to "tunnel" from one (deterministic locally stable) state to another. In this way, one stationary state generically "wins". Only if the parameters are changed fast enough, the picture changes and the hysteresis is present again (the tunneling effect is too slow). If the parameters are changed even faster, the hysteresis is destroyed, as the time scale separation of the change in the parameters and that in the system is not given any more.

References

[1] Th. Hillen, H. Othmer, *The diffusion limit of transport equations derived from velocity-jump processes*, SIAM J. Appl. Math. **61** (2001), 751–775.
[2] T. Lipniacki, P. Paszek, A. Mariciniak-Czochra, A.R. Basier, M. Kimmel, *Transcriptional stochasticity in gene expression*, J. Theor. Biol. **238** (2006), 348–367.
[3] J. Müller, Ch. Kuttler, B.A. Hense, S. Zeiser, V. Liebscher, *Transcription, intercellular variability and correlated random walk*, Math. Biosc. **216** (2008), 30–39.
[4] A.Raj, C. Peskin, D. Tranchina, D. Vargas, S. Tyagi, *Stochasticm RNA synthesis in mammalian cells*, PLoS Biol. **4**, (2006), 1707–1719.

Cell-based morphogenetic models

Markus Kirkilionis

We consider and discuss the mathematical structure of morphogenetic models based on a single cell or single cell nucleus framework. In particular we like to use structured cell population models, where the cells are structured according to their state in the cell-cycle, and any other necessary . To understand the mathematical structure in the following we start by looking at a typical single cell experiment, the movement of a single cell on a substrate in a Petri-dish. This basic experiment, for example changing the direction of motion of this cell under observation, shows the different structures we need to incorporate to understand the organization of multi-cell tissue models, see Fig. 1.

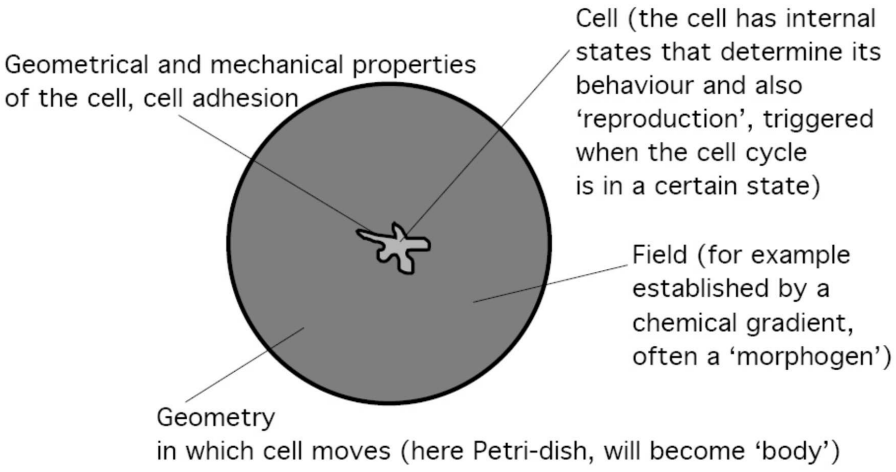

Figure 1. A cell in a cellular environment. According to current experimental knowledge cellular behaviour and growth will depend on the cell's internal state, the geometry of the external environment, positional information like chemical gradients (here called a 'field'), and the geometrical and mechanical properties of the cell itself.

It is clear that we need to structure any morphogenetic model with different detail taking all the aspects of Fig. 1 into account. The plan is to replace the classical reaction-diffusion models by cell-based at the same time internally and spatially structured cell populations. There are several reasons why this is required, both from a mathematical and an experimental point-of-view:

- The classical reaction-diffusion theory working with transport terms based on diffusion only, and deriving morphogen gradients with the help of Turing instabilities is not size-scale independent. As we know embryos even of the same species can vary in size considerably, such mechanisms cannot create robust developmental principles of self-organization.

- As a mathematical principle we therefore require a number of invariance principles all different classes of morphogenetic models have to satisfy. The most important one is that developmental dynamics should be independent of variations in embryo size. There are other such principles based on experimental evidence, for example using transplantation experiments and subsequent differentiation of the tissue. It has been suggested that transplantation experiments in morphogenesis cannot understood without memory of the system, here suggested to be equivalent to the cell's internal state.
- There is currently an explosion of data available for single cells, including the cell cycle which is essential to understand the differentiation and growth of tissues. In addition much more is known on how cell's interact and communicate with each other, for example by different receptors on the cell surfaces. To include such mechanisms structured cell populations are offering an ideal mathematical framework.

References

[1] M. Kirkilionis, *On the modelling of cellular interactions in tissues.*. In: Function and Regulation of Cellular Systems: Experiments and Models', A. Deutsch, Editor, Birkhuser, 2003.
[2] de Roos, A., Diekmann, O., Getto, P. and Kirkilionis, M., *Numerical equilibrium analysis for structured consumer resource models*, In press: Bulletin of Mathematical Biology, 2009.

Multi-species chemotaxis

Dirk Horstmann

Multi-agent-attraction resp. multi-agent-repulsion is nothing unusual in chemotaxis. There are several examples known for the reaction of mobile species to multiple stimuli in the environment. Furthermore, there are also examples where the chemotactical behavior of multiple population depends on the reaction to multiple attractants, like in host-parasitoid interactions. Taking all these aspects into account one can generalize the "classical" chemotaxis equations by Keller and Segel (compare [4]) to n mobile species that react on m different chemical substances. In this talk we consider the particular case of the following simplified multi-species system

$$
(1) \quad \begin{cases} \frac{\partial}{\partial t} p_i &= \nabla(k_{i,1}(p_i)\nabla p_i) + \nabla\left(\sum\limits_{l=1,l\neq i}^{n} \delta_{i,l} k_{i,2}(p_i)\theta_{i,l}(p_l)\nabla p_l\right) \\ & \quad -\nabla\left(\sum\limits_{j=1}^{m} \omega_{i,j} k_{i,3}(p_i)\nabla\Phi_{i,j}(s_j)\right), \ (x,t) \in \Omega \times (0,T) \\ \frac{\partial}{\partial t} s_j &= \left(\sum\limits_{k=1}^{m} b_{k,j}\Delta s_k\right) - \sum\limits_{k=1}^{m} \gamma_{k,j} f_{k,j}(s_k) + \sum\limits_{k=1}^{n} \alpha_{k,j} g_{k,j}(p_k, s_j), \\ & \quad (x,t) \in \Omega \times (0,T) \end{cases}
$$

with homogeneous Neumann boundary conditions, where the a_i, $b_{k,j}$, $\alpha_{k,j}$, $\omega_{i,j}$, $\delta_{i,l}$ and $\gamma_{k,j}$ are given constants and the $k_{i,1}(\cdot)$, $k_{i,2}(\cdot)$, $k_{i,3}(\cdot)$, $\theta_{i,l}$, $\Phi_{i,j}(\cdot)$, $f_{k,j}(\cdot)$ and

$g_{j,k}(\cdot,\cdot)$ are given functions. According to [5] we set $\lambda_{i,j} = \sum_{k=1}^{m} \omega_{i,k}\alpha_{j,k} = \omega_i\alpha_j$ if $k_{i,1}(\cdot) = id$, $k_{i,2}(\cdot) = id$, $k_{i,3}(\cdot) = id$, $\theta_{i,l} = 1$, $\Phi_{i,j}(\cdot) = id$, $f_{k,j}(\cdot) = id$ and $g_{j,k}(p,s) = p$. In this case G. Wolansky introduced in [5] the following notations:

(1) A population i_1 is attracted (resp. repelled) to (resp. from) a population i_2 if $\lambda_{i_1,i_2} > 0$ (resp. $\lambda_{i_1,i_2} < 0$). In particular, a population is self-attracting (self-repelling) if $\lambda_{i,i} > 0$ (resp $\lambda_{i,i} < 0$).

(2) A pair of populations $i_1, i_2 \in \{1, ..., n\}$ is said to be in a conflict, if $\lambda_{i_1,i_2} \times \lambda_{i_2,i_1} < 0$.

In the given situation a pair of populations $i_1, i_2 \in \{1, ..., n\}$ is said to be conflict-free, if $\lambda_{i_1,i_2} \times \lambda_{i_2,i_1} > 0$ and if there are n positive constants $\rho_1, ..., \rho_n$ such that $\rho_i\lambda_{i,l} = \rho_l\lambda_{l,j}$. However, for general systems like (1) we have to introduce also some other definitions (compare [1]):
Suppose that $k_{i,2}(\cdot)$ and $\theta_{i,j}(\cdot)$ do not change sign for all $i, j \in \{1, .., n\}$ with $i \neq j$. For $i \neq j$ we set $\kappa_{i,j}(p_i, p_j) = \delta_{i,j}k_{i,2}(p_i)\theta_{i,j}(p_j) \cdot \delta_{j,i}k_{j,2}(p_j)\theta_{j,i}(p_i)$.

(1) A population i_1 has common objectives (has no common objectives) with a population i_2 if $\kappa_{i_1,i_2}(p_{i_1}, p_{i_2}) > 0$ (resp. $\kappa_{i_1,i_2}(p_{i_1}, p_{i_2}) < 0$).

(2) If $\delta_{i_1,i_2}k_{i_1,i_2}(p_{i_1})\theta_{i_1,i_2}(p_{i_2}) = \delta_{i_2,i_1}k_{i_2,i_2}(p_{i_2})\theta_{i_2,i_1}(p_{i_1})$ we say that the populations i_1 and i_2 have homogeneous common objectives.

(3) We say that the system describes motion with common objectives, if and only if $\kappa_{i,j}(p_{i_1}, p_{i_2}) > 0$ for all $i, j \in \{1, ..., n\}$ with $i \neq j$.

Now we considered the special system

(2)
$$\begin{cases} \frac{\partial}{\partial t}p_i &= a_i\Delta p_i + \nabla\left[\sum\limits_{l=1,l\neq i}^{n} \delta_{i,l}p_i\nabla p_l - \sum\limits_{j=1}^{m} \omega_{i,j}p_i\nabla s_j\right],\ (x,t) \in \Omega \times (0,T) \\ \frac{\partial}{\partial t}s_j &= \left(\sum\limits_{k=1}^{m} b_{k,j}\Delta s_k\right) - \sum\limits_{k=1}^{m} \gamma_{k,j}s_k + \sum\limits_{k=1}^{n} \alpha_{k,j}p_k,\ (x,t) \in \Omega \times (0,T) \end{cases}$$

with homogeneous Neumann boundary conditions. Assuming additionally that the matrices $B = (b_{i,j})_{n\times n}$, $G = (\gamma_{i,j})_{m\times m}$ and $D = (\delta_{i,j})_{n\times n}$ are symmetric, B is positive definite and $\omega_{i,j} = 0$ iff $\alpha_{j,i} = 0$ for $i \in \{1, .., n\}$ and $j \in \{1, .., m\}$ holds true, we introduce (for this kind of conflict-free systems in the presence of motion with common objectives) the following Lyapunov functional:

$$\begin{aligned} L(\mathbf{p},\mathbf{s}) &= \frac{1}{2}\sum_{j=1}^{m}\sum_{l=1}^{m} \beta_{l,j} \int\limits_{\Omega} \left[b_{j,l}\nabla s_j\nabla s_l + \gamma_{j,l}s_js_l\right] dx + \sum_{i=1}^{n} \rho_i \int\limits_{\Omega} a_ip_i\log(p_i)dx \\ &\quad - \sum_{i=1}^{n}\sum_{j=1}^{m} \rho_i\omega_{i,j} \int\limits_{\Omega} p_is_j dx + \sum_{i=1}^{n}\sum_{k=1,k\neq i}^{n} \rho_i\delta_{i,k} \int\limits_{\Omega} p_ip_k dx, \end{aligned}$$

where the matrix $\beta = (\beta_{l,j})_{m\times m}$ is such that $\beta\alpha_i = \rho_i\omega_i$ for all $1 \leq i \leq n$ and $\sum\limits_{l=1}^{m} \beta_{l,j} > 0$ for all $j \in \{1, ..., m\}$ with $\rho_i > 0$ for all $i \in \{1, ..., n\}$. This generalizes a result in [5]. Now we see that $L(\mathbf{p},\mathbf{s})$ is monotone non-increasing for classical

solutions of (2) if $\rho_i > 0$ for all $i \in \{1, ..., n\}$, i.e. in the conflict-free situation. However, there are also other situations in which a Lyapunov functional exists. Therefore, we look at

(3)
$$\begin{cases} \frac{\partial}{\partial t} p_i &= \nabla(k_{i,1}(p_i, \mathbf{s})\nabla p_i) - \nabla\left(k_{i,2}(p_i, \mathbf{s}) \sum_{j=1}^{m} \omega_{i,j} \nabla s_j\right), \ (x,t) \in \Omega \times (0,T) \\ \frac{\partial}{\partial t} s_j &= \left(\sum_{k=1}^{m} b_{k,j} \Delta s_k\right) - \sum_{k=1}^{m} \gamma_{k,j} s_k + \sum_{k=1}^{n} \alpha_{k,j} g_{k,j}(p_k, s_j), \ (x,t) \in \Omega \times (0,T) \end{cases}$$

with homogeneous Neumann boundary conditions, where the $b_{k,j}$ and $\gamma_{k,j}$ are given constants and the functions $k_{i,1}(\cdot)$, $k_{i,2}(\cdot,\cdot)$ and $g_{k,j}(\cdot,\cdot) \neq 0$. Assuming the same as above for the matrices $B = (b_{i,j})_{n\times n}$, $G = (\gamma_{i,j})_{m\times m}$ and $D = (\delta_{i,j})_{n\times n}$, we set $G_{i,j}(p_i, s_j) = -\int^{s_j} g_{i,j}(p_i, y)dy$. As shown in [1] there exists a Lyapunov function for system (3), if there exist n functions $R_i(p_i)$ such that

$$\frac{k_{i,2}(p_i, \mathbf{s})}{k_{i,1}(p_i, \mathbf{s})} \left[\sum_{k=1}^{m} \omega_{i,k} \frac{\partial^2}{\partial p_i^2} G_{i,k}(p_i, s_k) + \frac{d^2}{dp_i^2} R_i(p_i)\right] + \frac{\partial^2}{\partial p_i \partial s_j} G_{i,j}(p_i, s_j) = 0$$

for all $j \in \{1, ...m\}$ if additionally

$$\sum_{j=1}^{m} \frac{\partial^2}{\partial p_i^2} G_{i,j}(p_i, s_j) + \frac{d^2}{dp_i^2} R_i(p_i) \geq 0 \text{ for all } i \in \{1, ..., n\}$$

holds true for the solution of (3). The Lyapunov function for system (3) is then given by

$$\begin{aligned} H(\mathbf{p}, \mathbf{s}) &= \frac{1}{2} \sum_{j=1}^{m} \sum_{l=1}^{m} \int_{\Omega} \beta_{l,j} \left[b_{j,l} \nabla s_j \nabla s_l + \gamma_{j,l} s_j s_l\right] dx + \sum_{i=1}^{n} \int_{\Omega} \rho_i R_i(p_i) dx \\ &\quad + \sum_{i=1}^{n} \sum_{j=1}^{m} \rho_i \omega_{i,j} \int_{\Omega} G_{i,j}(p_i, s_j) dx, \end{aligned}$$

if $\rho_i > 0$ for all $i \in \{1, ..., n\}$, where the matrix $\beta = (\beta_{l,j})_{m\times m}$ is such that $\beta\alpha_i = \rho_i\omega_i$ for all $1 \leq i \leq n$ and $\sum_{l=1}^{m} \beta_{l,j} > 0$ for all $j \in \{1, ..., m\}$.

In the last part of the talk, we paid our attention to some simplified multi-species chemotaxis models that (after some transformations) are of the following type:

$$(4) \quad \begin{cases} U_t &= \nabla(\nabla U - \chi_1 U \nabla V), & \text{in } \Omega \times (0,T) \\ W_t &= \nabla(\nabla W \pm \chi_2 W \nabla V), & \text{in } Q_T \\ V_t &= \Delta V - \gamma V + \nu^{\pm}\left(\lambda U \pm \mu W - \frac{1}{|\Omega|}\right), & \text{in } \Omega \times (0,T) \\ \frac{\partial U}{\partial n} &= \frac{\partial W}{\partial n} = \frac{\partial V}{\partial n} = 0 & \text{on } \Gamma_T \\ U(0,x) &= U_0(x), \ W(0,x) = W_0(x), & x \in \Omega, \\ V(0,x) &= V_0(x), & x \in \Omega. \end{cases}$$

As mentioned before, we have two Lyapunov functionals at hand in the conflict-free situations that are helpful tools for analyzing the time asymptotic behavior

of the solutions. The corresponding steady state problems to (4) are given by:

$$0 = \Delta V - \gamma V + \nu^{\pm}\left(\lambda\frac{e^{\chi_1 V}}{\int\limits_\Omega e^{\chi_1 V}dx} \mp \mu\frac{e^{\mp\chi_2 V}}{\int\limits_\Omega e^{\mp\chi_2 V}dx} - \frac{1}{|\Omega|}\right) \tag{5}$$

and have a variational structure. Besides some statements on the time asymptotic behavior of solutions to (4) also some existence and uniqueness results for problem (5) are established by using some results from [3].

References

[1] D. Horstmann, *Generalzing Keller-Segel: Multi-species chemotaxis models with attraction and repulsion between competitive, interacting species*, submitted.

[2] D. Horstmann and M. Lucia, *Symmetry and uniqueness of equilibria in a chemotaxis model*, submitted.

[3] D. Horstmann, M. Lucia, *Nonlocal elliptic boundary value problems related to chemotactic movement of mobile species*, submitted.

[4] E. F. Keller, L. A. Segel, Initiation of slime mold aggregation viewed as an instability,*J. Theor. Biol.* **26** (1970), 399–415.

[5] G. Wolansky, *Multi-components chemotactic system in absence of conflicts*, Euro. Jnl. of Applied Mathematics **13** (2002), pp. 641 – 661.

Measure solutions of the 2D Keller-Segel model as limit of a stochastic many particle model

Christian Schmeiser

(joint work with Jan Haskovec)

The existence theory of strong solutions of the two-dimensional elliptic-parabolic Keller-Segel model

$$\partial_t\rho + \nabla\cdot(\rho\nabla S[\rho] - \nabla\rho) = 0\,,$$
$$S[\rho](x) = -\frac{1}{2\pi}\int_{\mathbb{R}^2}\log(|x-y|)\rho(y)\,dy\,,$$

subject to the initial condition $\rho(t=0)=\rho_I$, has reached a very mature state recently. Already in [6] it has been observed that the total mass $M = \int_{\mathbb{R}}\rho\,dx$ of the cells is a critical parameter. For solutions with bounded second moment ($\int_{\mathbb{R}}\rho|x|^2\,dx < \infty$), strong solutions exist globally in time in the subcritical case $M < 8\pi$, and the cell population is dispersed. In the supercritical case $M > 8\pi$ solutions blow up in finite time creating point aggregates of cells, and in the critical case $M = 8\pi$ solutions exist globally in time and aggregate in infinite time [1], [2]. In [3] Poupaud's theory of diagonal defect measures [7] has been applied to prove unconditional global existence of weak measure solutions of the generalized problem

$$\partial_t\rho + \nabla\cdot(j[\rho,\nu] - \nabla\rho) = 0\,,$$

where $\nu \in \mathcal{M}_1((0,T)\times\mathbb{R}^2)^{2\times 2}$ is a symmetric, nonnegative matrix valued measure (the so-called *diagonal defect measure*), verifying the estimate

$$\mathrm{tr}(\nu(t,x)) \le \sum_{a\in S_{at}(\rho(t))} \rho(t)(\{a\})^2\delta(x-a)\,,$$

with $S_{at}(\rho(t))$ denoting the atomic support of the limiting bounded, nonnegative Radon measure $\rho(t) \in \mathcal{M}_1^+(\mathbb{R}^2)$. The distributional definition of the convective flux $j[\rho,\nu]$ with a test function $\phi \in C_c^\infty((0,T),\mathbb{R}^2)$ is given by

$$\begin{aligned}&\int_0^T \int_{\mathbb{R}^2} j[\rho,\nu](t,x)\phi(t,x)dx\,dt\\ &= -\frac{1}{2}\int_0^T \int_{\mathbb{R}^4} \mathcal{K}(x-y)\rho(t,x)\rho(t,y)(\phi(t,x)-\phi(t,y))\,dx\,dy\,dt\\ &\quad -\frac{1}{2}\int_0^T \int_{\mathbb{R}^2} \nu(t,x)\nabla\phi(t,x)\,dx\,dt\,,\end{aligned}$$

with $\mathcal{K}(x) = \frac{x}{2\pi|x|^2}$ for $x \neq 0$, and $\mathcal{K}(0) = 0$.

In the spirit of [8] the Keller-Segel problem can been approximated by the system

$$dx_n = -\frac{M}{N}\sum_{n\neq m\le N} \mathcal{K}^\varepsilon(x_n - x_m)dt + \sqrt{2}\,dB^n\,, \quad \mathcal{K}^\varepsilon(x) = \frac{x}{|x|(|x|+\varepsilon)}\,,$$

of stochastic differential equations for a system of N identical particles with mass M/N. The regularization parameter $\varepsilon > 0$ is used to make the deterministic particle velocity bounded. This is sufficient for existence and uniqueness of bounded solutions of the corresponding Kolmogorov forward equation

$$\partial_t p + \sum_{n=1}^N \nabla_{x_n}\cdot\left(-\frac{M}{N}\sum_{m\neq n}\mathcal{K}^\varepsilon(x_n-x_m)p - \nabla_{x_n}p\right) = 0\,, \tag{1}$$

for the many-particle probability distribution $p = p(t,x_1,\dots,x_N)$. In [4] the limit $N\to\infty$ has been carried out for fixed positive ε and initial conditions $p(0,x_1,\dots,x_N) = P_I(x_1)\cdots P_I(x_N)$ of i.i.d. particles. As a result, global solutions of a regularized Keller-Segel problem are derived, which, by the theory of [3], converge to measure valued solutions as $\varepsilon\to 0$.

The order of the limits has been reversed in [5]. The limit $\varepsilon\to 0$ in (1) leads to measure solutions with diagonal defect measures similarly to the Poupaud theory. Subsequently, also the limit $N\to\infty$ can be carried out with the (distributional) convergence result

$$\lim_{N\to\infty}\int_{\mathbb{R}^{2(N-k)}} p\,dx_{k+1}\dots dx_N = P(t,x_1)\cdots P(t,x_k)$$

for marginals, where $MP(t,x)$ is a measure solution (with diagonal defect measure) of the Keller-Segel model. A similar factorization property holds for the limiting defect measures.

References

[1] A. Blanchet, J.A. Carrillo, N. Masmoudi, *Infinite time aggregation for the critical Patlak-Keller-Segel model in* $\mathbb{R}^2$, Commun. Pure Appl. Math. **61** (2008), 1449–1481.

[2] A. Blanchet, J. Dolbeault, B. Perthame, *Two-dimensional Keller-Segel model: optimal critical mass and qualitative properties of the solutions*, Electr. J. Diff. Equ. **2006** (2006), No. 44, 1–33.

[3] J. Dolbeault, C. Schmeiser, *The two-dimensional Keller-Segel model after blow-up*, to appear in DCDS-A, 2009.

[4] J. Haskovec, C. Schmeiser, *Stochastic particle approximation to the global measure valued solutions of the Keller–Segel model in 2D*, J. Stat. Phys. **135** (2009), 133–151.

[5] J. Haskovec, C. Schmeiser, in preparation (2009).

[6] W. Jäger, S. Luckhaus, *On explosions of solutions to a system of partial differential equations modelling chemotaxis*, Trans. Amer. Math. Soc. **329** (1992), 819–824.

[7] F. Poupaud, *Diagonal defect measures, adhesion dynamics and Euler equations*, Meth. Appl. Anal. **9** (2002), 533–561.

[8] A. Stevens, *The derivation of chemotaxis equations as limit dynamics of moderately interacting stochastic many-particle systems*, SIAM J. Appl. Math. **61** (2000), 183–212.

Non unique continuation of solutions of the Keller-Segel model in the sense of measures

Juan J. L. Velazquez

(joint work with S. Luckhaus, Y. Sugiyama)

The classical Keller-Segel model for chemotactic aggregation in two spatial dimensions reads as:

$$\begin{aligned} u_t &= \Delta u - \nabla (u \nabla v) \\ 0 &= \Delta v + u \end{aligned}$$

It is well known that the solutions of this PDE can develop singularities in finite time (cf. [1]). Moreover, a large amount of information concerning the number of possible blow-up points and the structure of the solutions at the time of formation of the singularities is known (cf.[4]).

In this report, the continuation of the solutions beyond the blow-up time is considered. It turns out that the resulting weak solutions derived in this form satisfy different weak formulations that generalize the concept of solution for the Keller-Segel system to measure valued solutions.

The continuation of the solutions of the Keller-Segel system beyond the blow-up time has been considered in several papers and with different approaches. In the paper [5] the following system was studied using formal asymptotic expansions:

$$\begin{aligned} u_t &= \Delta u - \nabla\left(f_\varepsilon\left(u\right)\nabla v\right) \\ 0 &= \Delta v + u \\ f_\varepsilon\left(u\right) &= \frac{1}{\varepsilon}F\left(\varepsilon u\right) \ , \ \varepsilon > 0 \\ F\left(U\right) &= \frac{1}{1+U} \end{aligned}$$

In particular, it was seen in [5] that the solutions of this regularized system of equations should converge to a measure having the form:

$$u = \sum_j \alpha_j\left(t\right)\delta_{x_j(t)} + u_{reg}$$

where $\alpha_j\left(t\right),\ x_j\left(t\right)$ satisfy a system of ODEs coupled with the evolution of the regular part of this measure.

A different approach was used in [3]. In this paper a concept of weak solution that allowed to extend the concept of solution for the Keller-Segel model to measures was introduced. A key step in the definition of weak solution used in [3] was a symmetrization argument of the nonlinear term rather similar to the argument used in the paper [4] to prove single point blow-up for the Keller-Segel system.

We have considered in the paper [2] two different regularizations of the Keller-Segel system, namely:

$$\begin{aligned} u_t &= \Delta u - \nabla\left(f_\varepsilon\left(u\right)\nabla v\right) \\ 0 &= \Delta v + f_\varepsilon\left(u\right) \\ f_\varepsilon\left(u\right) &= \frac{1}{\varepsilon}F\left(\varepsilon u\right) \ , \ \varepsilon > 0 \\ F\left(U\right) &= \frac{1}{1+U} \end{aligned}$$

and

$$\begin{aligned} u_t &= \Delta\left(u + \varepsilon u^\alpha\right) - \nabla\left(u\nabla v\right) \ , \ \alpha > 1 \ , \ \varepsilon > 0 \\ 0 &= \Delta v + u \end{aligned}$$

We prove in [2] that the limit of the solutions of these two different systems converge to different measures that satisfy different weak formulations. Moreover, we obtain information on the amount of mass that can be concentrated at the singular points for both limit measures.

References

[1] W. Jaeger and S. Luckhaus *On explosions of solutions to a system of partial differential equations modelling chemotaxis.* Trans. Amer. Math. Soc. **329**, 2 (1992), 819-824.

[2] S. Luckhaus, Y. Sugiyama and J.J.L.Velazquez, Non unique continuation of solutions of the Keller-Segel model in the sense of measures. In preparation.

[3] F. Poupaud, Diagonal defect measures, adhesion dynamics and Euler equation. Methods. Appl. Anal. 9, n.4, 533-561, (2002).

[4] T. Senba and T. Suzuki *Chemotactic collapse in a parabolic-elliptic system of mathematical biology.* Advances in Differential Equations. **6**, 1 (2001), 21-50.
[5] J. J. L. Velzquez, Point dynamics for a singular limit of the Keller-Segel model. I. Motion of the concentration regions. SIAM J. Appl. Math. 64, 4, 1198-1223, (2004).

Some kinetic models in swarming

José A. Carrillo

I presented a kinetic theory for swarming systems of interacting, self-propelled discrete particles. Starting from the the particle model [6], one can construct solutions to a kinetic equation for the single particle probability distribution function using distances between measures [5].

Moreover, I introduced related macroscopic hydrodynamic equations. General solutions include flocks of constant density and fixed velocity and other non-trivial morphologies such as compactly supported rotating mills. The kinetic theory approach leads us to the identification of macroscopic structures otherwise not recognized as solutions of the hydrodynamic equations, such as double mills of two superimposed flows.

I also presented and analysed the asymptotic behavior of solutions of the continuous kinetic version of flocking by Cucker and Smale [4], which describes the collective behavior of an ensemble of organisms, animals or devices. This kinetic version introduced in [7] is obtained from a particle model. The large-time behavior of the distribution in phase space is subsequently studied by means of particle approximations and a stability property in distances between measures. A continuous analogue of the theorems of [4] was shown to hold for the solutions on the kinetic model. More precisely, the solutions concentrate exponentially fast their velocity to their mean while in space they will converge towards a translational flocking solution.

The presentation was based in works in collaboration [1, 2, 3].

References

[1] J. A. Carrillo, J. A. Cañizo and J. Rosado. Well-posedness of the swarming equations in the space of measures, work in preparation.
[2] J. A. Carrillo, M. R. D'Orsogna and V. Panferov. Double milling in self-propelled swarms from kinetic theory, to appear in *Kinetic and Related Models*.
[3] J. A. Carrillo, M. Fornasier, J. Rosado and G. Toscani. Asymptotic Flocking Dynamics for the kinetic Cucker-Smale model, preprint.
[4] F. Cucker and S. Smale. Emergent behavior in flocks. *IEEE Trans. Automat. Control*, **52** (2007), 852–862.
[5] R. Dobrushin. Vlasov equations. *Funct. Anal. Appl.*, **13** (1979), 115–123.
[6] M.R. D'Orsogna, Y.-L. Chuang, A. L. Bertozzi, L. Chayes. Self-propelled particles with soft-core interactions: patterns, stability, and collapse. *Phys. Rev. Lett.*, **96** (2006), 104302-1/4.
[7] S.-Y. Ha and E. Tadmor. From particle to kinetic and hydrodynamic descriptions of flocking. *Kinetic and Related Models*, **1** (3) (2008), 415-435.

Qualitative behavior of a Keller-Segel model with non-diffusive memory

Kyungkeun Kang
(joint work with Angela Stevens, Juan J. L. Velázquez)

We consider a one-dimensional Keller-Segel model with a logarithmic chemotatic sensitivity and a non-diffusion chemical:

$$u_t = u_{xx} - \left(u\frac{w_x}{w}\right)_x, \qquad w_t = uw^\lambda, \qquad 0 \le \lambda < 1. \tag{1}$$

The main question addressed for the equations (1) is whether smooth solutions exist globally in time, or blowup happens. A crucial assumption is that the chemical is produced by the chemotactic species and decay terms do not occur. The equations (1) was introduced and formally analyzed in [3] and [2], respectively.

Using the change of variable, $z = (1-\lambda)^{-1}w^{\frac{1}{\theta}}$ with $\theta = \frac{1}{1-\lambda}$, the equation (1) can be written as

$$u_t = u_{xx} - \theta\left(u\frac{z_x}{z}\right)_x, \qquad z_t = u, \qquad 1 \le \theta < \infty. \tag{2}$$

In [4], existence of global solutions for linear production kinetics, $\lambda = 0$(or $\theta = 1$) was proved. On the other hand, it was shown in [1] that finite time blow-up may occur for specific explicit initial data provided that production kinetics are exponential, $\lambda = 1$ (or $\theta = \infty$).

We note that (a, at) with $a > 0$ is a spatially independent solution of (2). In case that $\theta = 1$, we show both linear and nonlinear stability for solutions of (2) when initial data of the solutions is sufficiently close to the homogeneous solution. To be more precise, we prove

Theorem I Let $\theta = 1$ and (a, at) be a space-independent solution of (2), where $a > 0$ is constant. If (u, z) is a solution with initial data (u_0, z_0) sufficiently close to (a, a), then there exists $v_\infty \in H^2$ such that u and $\frac{z}{t}$ both converges to $a + v_\infty$ for $t \to \infty$ in a suitable sense. □

For the proof of Theorem I we use the Fourier expansions. We first look for solution of the form

$$u(x,t) = a + v(x,t), \qquad z(x,t) = at + \xi(x,t).$$

We then obtain the perturbed equations

$$v_t = v_{xx} - \left(\frac{1}{t}\zeta_x\right)_x - \left(\frac{\zeta_x}{\bar{z}+\zeta}v - \frac{a\zeta\zeta_x}{\bar{z}(\bar{z}+\zeta)}\right)_x, \qquad \zeta_t = v.$$

For convenience, we introduce the norm $|||\psi|||^2_{L,k} = \int_{(L-1)^+}^{L} ||\psi(t)||^2_{H^k} dt$, where $k \ge 0$, $L > 1$ and $(L-1)^+ = \max\{L-1, 1\}$. We treat separately the stability issues for linear or nonlinear case and the convergence of u and $\frac{z}{t}$ to $a + v_\infty$ for $t \to \infty$ for both cases can be shown in the following sense, respectively:

(i) (Stability of the linearized case)

$$||u(t) - (a + v_\infty)||_{H^2} \longrightarrow 0, \quad \text{as } t \to \infty,$$

$$\left|\left|\frac{\zeta(t)}{t} - (a + v_\infty)\right|\right|_{H^2} \longrightarrow 0 \quad \text{as } t \to \infty.$$

(ii) (Stability of the nonlinear case)

$$\left|\left|\frac{\zeta(t)}{t} - v_\infty\right|\right|_{H^2} \longrightarrow 0 \quad \text{for } t \to \infty,$$

$$||v(t) - v_\infty||_{H^1} \longrightarrow 0 \quad \text{for } t \to \infty,$$

$$|||v - v_\infty|||_{L,2} \longrightarrow 0 \quad \text{for } L \to \infty.$$

On the other hand, in case that $1 < \theta < 3$, we construct blow up solutions at infinite time. More precisely, we prove the following:

Theorem II There exist a family of initial data $u_0, z_0 \in \mathcal{C}^{2,\nu}$ such that the corresponding solutions (u, z) of (2) satisfy $u(x,t) \to \mu\delta(x)$ in the sense of measures, where $\mu = \int_I u_0(x)dx$. Moreover, the following asymptotic formula hold for $z(x,t)$:

(i) $z(x,t) \to z_\infty(x)$ as $t \to \infty$ uniformly in compact sets of $I \setminus \{0\}$ for some function $z_\infty \in \mathcal{C}^2(I \setminus \{0\})$ satisfying $\lim_{x\to\infty} x^{\frac{2}{\theta-1}} z_\infty(x) = B^{-\frac{1}{\theta-1}}$.

(ii) There exist constants A, B depending on the initial data such that

$$\lim_{t\to\infty} \frac{z\left(\frac{y}{t^{\frac{\theta-1}{3-\theta}}}, t\right)}{t^{\frac{2}{3-\theta}}} = \frac{1}{(By^2 + A)^{\frac{1}{\theta-1}}}$$

uniformly in any compact sets $\{y : |y| \le C\}$. □

References

[1] H. Levine & B. Sleeman *A system of reaction diffusion equations arising in the theory of reinforced random walks.* SIAM J. Appl. Math **57** (1997), no. 3, 683–730.

[2] H. G. Othmer & A. Stevens *Aggregation, blowup, and collapse: the ABC's of taxis in reinforced random walks.* SIAM J. Appl. Math.

[3] A. Stevens *Trail following and aggregation of myxobacteria.* J. of Biol. Systems **3** (1995), 1059–1068.

[4] Y. Yang, H. Chen & W. Liu *On existence of global solutions and blow-up to a system of reaction diffusion equations modelling chemotaxis*, SIAM J. Math. Anal. **33** (2001), no. 4, 763-785.

The delay equation formulation of structured population models

Odo Diekmann
(joint work with Mats Gyllenberg, Hans Metz)

A delay equation is a rule for extending a function of time towards the future, on the basis of the known past. Renewal Equations prescribe the current value, while Delay Differential Equations prescribe the derivative of the current value. With a delay equation one can associate a dynamical system by translation along the extended function. There is a rich qualitative theory for these dynamical systems.

Structured population models are traditionally formulated as first order PDE with non-local boundary conditions. By way of two examples (size-structured consumers competing for an unstructured resource and size-structured cell populations) we show how, for a special class of initial conditions, these models can be reformulated in terms of delay equations. The special class forms a forward invariant attracting set, so the information that is lost by restricting to it concerns transient behaviour only.

The consumer-resource model is described by the system

$$
\begin{aligned}
b(t) &= \int_0^\infty b(t-a)\ \beta(\Xi(a;S_t),S(t))\mathcal{F}(a;S_t)da,\\
\frac{dS}{dt}(t) &= f(S(t)) - \int_0^\infty b(t-a)\gamma(\Xi(a;S_t),S(t))\mathcal{F}(a;S_t)da.
\end{aligned}
\tag{1}
$$

It is extensively studied in a joint paper with Mats Gyllenberg, Shinji Nakaoka, Hans Metz and Andre de Roos. This paper, entitled Daphnia revisited, is dedicated to Horst Thieme at the occasion of his 60th birthday.

Equations with infinite delay

Mats Gyllenberg
(joint work with Odo Diekmann)

A large class of models of physiologically structured populations take the form of a nonlinear renewal equation coupled with a delay-differential equation:

$$x(t) = F_1(x_t, y_t), \tag{1}$$

$$\dot{y}(t) = F_2(x_t, y_t), \quad t > 0. \tag{2}$$

Here the unknowns x and y are defined on $\mathbb{R}$ with values in $\mathbb{R}^m$ and $\mathbb{R}^n$, respectively. The subscript denotes translation:

$$x_t(\theta) := x(t+\theta), \quad -\infty < t \leq 0.$$

The equations (1) and (2) have to be supplemented by initial conditions

$$x(t) = \varphi(t), \tag{3}$$

$$y(t) = \psi(t), \quad -\infty < t \leq 0. \tag{4}$$

Let $\varrho > 0$. As state space we choose $X = X_1 \times X_2$ with $X_1 = L^1_\varrho(\mathbb{R}_-;\mathbb{R}^m)$, the Banach space of all (equivalence classes of) measurable functions $\varphi : \mathbb{R}_- = (-\infty, 0] \to \mathbb{R}^m$ such that the weighted integral

$$\|\varphi\|_{1,\varrho} = \int_{-\infty}^{0} e^{\varrho\theta}|\varphi(\theta)|\,d\theta \tag{5}$$

is finite, and $X_2 = C_{0,\varrho}(\mathbb{R}_-;\mathbb{R}^n)$ of all $\mathbb{R}^m$-valued functions ψ defined on $\mathbb{R}_-$ such that $\theta \mapsto e^{\varrho\theta}\psi(\theta)$ is continuous and vanishes at minus infinity with norm

$$\|\psi\|_{\infty,\varrho} = \sup_{\theta\in\mathbb{R}_-} e^{\varrho\theta}|\psi(\theta)|.$$

The function F_1 maps X into $\mathbb{R}^m$ and F_2 maps X into $\mathbb{R}^n$.

A first reason for the weight is that we want to consider *steady-states* , that is, constant solutions of (1) & (2), and constants do not belong to L^1 when the domain (delay) is infinite. The second reason for the weight is that we want some Laplace transforms to be defined in a strip to the left of the imaginary axis.

Assume that F is continuouslu Fréchet differebtiable. Linearizing the concrete system (1) & (2) about a steady-state one obtains

$$x(t) = \int_0^\infty k_{11}(\theta)x(t-\theta)d\theta + \int_{\mathbb{R}_+} \mu_{12}(d\theta)y(t-\theta), \tag{6}$$

$$\dot{y}(t) = \int_0^\infty k_{21}(\theta)x(t-\theta)d\theta + \int_{\mathbb{R}_+} \mu_{22}(d\theta)y(t-\theta), \tag{7}$$

where k_{11} and k_{21} are matrix valued functions defined on $\mathbb{R}_+$ such that

$$\|k_{i1}\|_{\infty,\varrho} < \infty$$

and μ_{12} and μ_{22} are matrices, the elements of which are measures on $\mathbb{R}$ such that

$$\int_{\mathbb{R}_+} e^{\varrho\theta}\mu(d\theta) < \infty.$$

Let

$$M(\lambda) = \begin{pmatrix} I & 0 \\ 0 & \lambda I \end{pmatrix} - \begin{pmatrix} \widehat{k}_{11}(\lambda) & \widehat{\mu}_{12}(\lambda) \\ \widehat{k}_{21}(\lambda) & \widehat{\mu}_{22}(\lambda) \end{pmatrix},$$

where the hat denotes Laplace transform. The *characteristic equation* is

$$\det M(\lambda) = 0. \tag{8}$$

In [3] we proved the following theorem.

Theorem 0.1. (Principle of linearized stability)

(a) *If all the roots of the characteristic equation* (8) *have negative real part, then the steady state is exponentially stable.*

(b) *If there exists at least one root of* (8) *with positive real part, then the steady state is unstable.*

Theorem 0.1 extends the results of [5] to the case of infinite delay. As in [5], we use perturbation theory of adjoint semigroups to prove Theorem 0.1. In fact, we show that the concrete problem (1) & (2) is equivalent to the abtract integral equation

$$u(t) = T_0(t) \begin{pmatrix} \varphi \\ \psi \end{pmatrix} + j^{-1} \int_0^t T_0'^*(t-s)(\ell \circ F)(u(s))ds. \tag{9}$$

Here the unperturbed semigroup T_0 is shift to the left and extension by zero in the first component and by the value at zero in the second component. $T_0'^*$ is an extension of T_0 to a bigger space X'^* and j is a natural injection of X into X'^*. ℓ is an injection of $\mathbb{R}^m \times \mathbb{R}^n$ into X'^*.

In the case of finite delay the problem has a property called *sun-reflexivity*, which, amoing other things, guarantees that the integral in (9) makes sense and belongs to $j(X)$. However, a small modification of the sun-reflexive theory makes it possible to treat equations with infinite delay in essentially the same framework.

Lack of compactness is a second complication that arises when one moves from finite to infinite delay. When the delay h is finite, the unperturbed semigroup $T_0(t)$ will have finite dimensional range for $t > h$. In applications to renewal equations it is even nilpotent. In any case, T_0 is eventually compact when the delay is finite. Combined with the fact that G has finite dimensional range, this yields that the perturbed semigroup T for the linearized equation is eventually compact. As a consequence, the spectrum of the infinitesimal generator A of T is a pure point spectrum and the growth bound $\omega(T)$ of T equals the spectral bound $s(A)$ of A, which is the supremum of the real part of the eigenvalues of A. It follows that to determine the stability or instability of steady-states it suffices to locate the eigenvalues of A in the complex plane. When the delay is infinite, this is no longer necessarily true and the inequality $s(A) \leq \omega(T)$ may be strict. Therefore the location of the eigenvalues of A does not tell the whole story. But here we switch from the abstract setting to the concrete delay equations and use the Payley-Wiener theorem.

References

[1] O. Diekmann and M. Gyllenberg, Abstract delay equations inspired by population dynamics, In *Functional Analysis and Evolution Equations,* H. Amann, W. Arendt, M. Hieber, F. Neubrander, S. Nicaise, J. von Below (Eds.), Birkhäuser (2007) pp. 187-200.

[2] O. Diekmann M. and Gyllenberg, The second half - with a quarter of a century delay, Mathematical Modelling of Natural Phenomena 3 (2008) 36-48.

[3] O. Diekmann and M. Gyllenberg, *Equations with infinite delay: blending the abstract and the concrete,* Journal of Differential Equations, submitted.

[4] O. Diekmann, S.A. van Gils, S.M. Verduyn Lunel and H.-O. Walther, "Delay Equations. Functional-, Complex-, and Nonlinear Analysis," Springer-Verlag, New York 1995.

[5] O. Diekmann, Ph. Getto, M. Gyllenberg, *Stability and bifurcation analysis of Volterra functional equations in the light of suns and stars.* SIAM Journal on Mathematical Analysis, **39** (2007) 1023-1069.

[6] O. Diekmann, M. Gyllenberg, J.A.J. Metz, S. Nakaoka, and A.M. de Roos, *Daphnia revisited: local stability and bifurcation theory for physiologically structured population models explained by way of an exmple,* Journal of Mathematical Biology, submitted.

Model supported data analysis – some examples and principles

Wolfgang Alt

A historical review, which seems appropriate in the current DARWIN-year celebrating the initiation of modern evolution theory 150 years ago, reveals that *"Mathematical Biology"* with the Oberwolfach Conferences having been started in 1975 can look back to an age of almost one century, thinking of LOTKA's seminal work in 1925, for example, and the subsequent initiation of *"Population Genetics"*, whose roots go further back to the early bio-statistical ('biometric') theories by PEARSON in the beginning of the 20th century, when also the concept of 'gene' was coined – 1909, exact 100 years ago [1]. In the same year, the zoologist UEXKÜLL, who together with the botanist REINKE was one of the early founders of *"Theoretical Biology"* [2], had coined the theoretical concept of environment ('Umwelt') as the exterior 'counter-part' of the interior dynamic structure ('Gefüge) of a living organism, experienced by applying various 'functional cycles of action and perception': each organism constructs its own 'Umwelt' as world of acting ('Wirkwelt') and world of sensing ('Merkwelt') in such a way that any object only appears as a counter-structure ('Gegengefüge') between internally represented action signals ('Wirkmale') and sensor signals ('Merkmale'). Thereby the 'outer feedbacks' of an own action via perceived environmental signals can be functionally controlled ('counter-rolled') by 'inner feedback cycles' as realized by the neural feedback of proprioception during locomotion.

By presenting three biological examples I want to prove and emphasize, that this quite simple but important 'principle of life' has to be regarded, when mathematical models are used to analyse and interpret the observations of living organisms. Often, essentially 'descriptive' models are applied, which by numerical simulation, statistical analysis and parameter fitting just want to reproduce the experimental data as they have been acquired and measured by the observer. However, then we can easily fail by not primarily modeling the organism, rather our own cognitive process of experimenting and observing. Thus, a true **biological model supported data analysis** must try to reconstruct the internal 'knowledge' and 'functional regulation', which the organism uses to perform the behavior that we observe.

0.1. **Orientation and path integration in desert ants.** Desert ants as *Cataglyphis fortis* use a hitherto unknown neural algorithm of path integration for estimating the position of their nest (='home') relative to their current body axis, by using quite accurate measurements of their walking speed $v(t)$ and angular orientation, thus also of their turning speed $\omega(t)$. Nevertheless, one observes systematic errors of their homing path with a tendency to underestimate the distance in proportion to the length of the outgoing path and to overestimate the orientation angle in proportion to its net curvature. A simple model of 'leaky integration' is proposed [4], which implements a constant leakage rate into the activity of two hypothetical interneurons representing the current values of the ant's egocentric Cartesian coordinates $(X(t), Y(t))$ for nest position, see Fig. 1(left). The observed

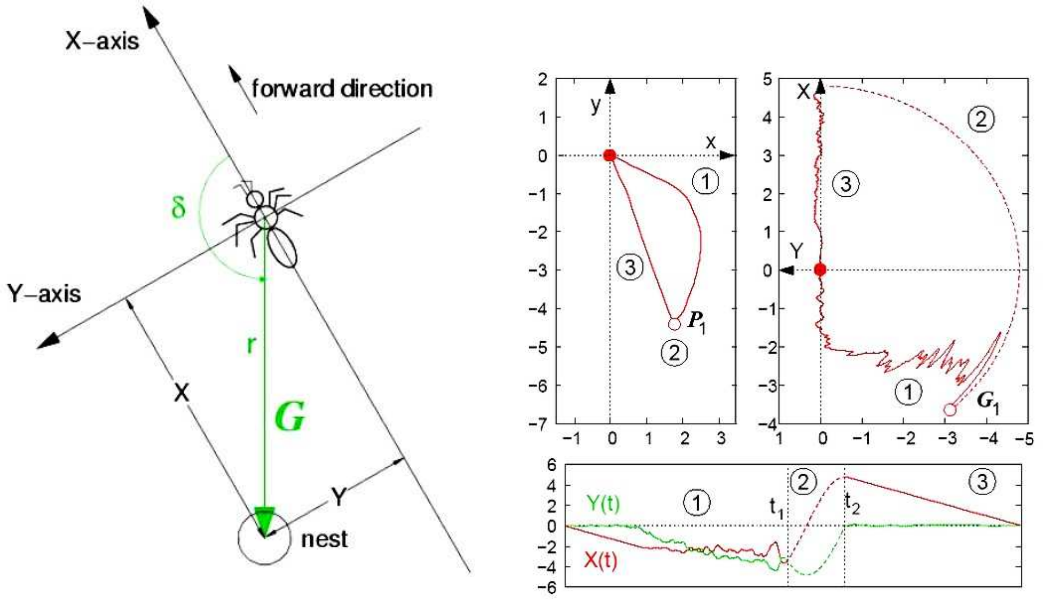

FIGURE 1

geocentric coordinates $(x(t), y(t))$ of the ant's moving path is then transformed via a simple linear ODE for (X, Y) with v and ω as coefficients, whose solution could easily be realized by the ant's brain. See Fig. 1(right) for visualization of a simulated path during foraging (1), reorientation (2) and homing (3), showing totally different trajectories in the observer's and the ant's view. Though other models, which rely on an artificial approximation of the nonlinearities appearing in the path integrator ODE for egocentric polar coordinates, can also reproduce the observed orientation data, we strongly argue for the more physiological 'leaky integrator' model, whose outcome might even be 'anticipated' by the ant and used as information for further phases of systematic home search. When statistically analysing the field data of ant paths (recorded in the Tunesian desert) under support of our model, three internal control parameters can be extracted: the leakage parameter for path integration, the strength as well as the time constant for counter-steering of the turning rate $\omega(t)$ in response to the internally represented 'sidewards nest deviation' $Y(t)$ on the way home.

0.2. **Burst response of neuromast sensor cells.** Fishes as the goldfish *Carassius auratus* use the lateral line system to measure relative speeds or pressure differences of the surrounding water by mechanosensors called neuromast. Not only in response to such stimuli, also spontaneously, extracellular recordings of single neuromasts reveal characteristic features of bursting spike sequences (action potentials in the axonal plasma membrane). Whereas the statistical analysis of Poisson-like burst processes is usually performed by investigating the distribution or correlation of the observed interval times, we propose a general method of model supported burst analysis regarding the above-mentioned 'life principle': Within the neural network of post-sensor data processing by the fish brain, at the

synapses any presynaptic spike train signal S_t is transformed into a non-spiking postsynaptic membrane depolarization $P(t)$, which can be reconstructed by solving the simple differential equation $dP = S_t - P * dt/T$ (linear filter of 1^{st} order) driven by the empiric signal as stochastic input. Then, standard probability theory and auto-correlation analysis can be applied to extract characteristic properties of the neuromast bursting pattern. Moreover, we realize that 'integrate-and-fire' models for spike burst generation at the axon hill of a single sensor or neuron cell (cf. [5]) assume analogous types of differential equations for inhibiting membrane currents $R(t)$ as 'negative feedback' onto the own membrane potential, and therefore might regard this as a kind of 'proprioceptive functional cycle', thus as a part of the cell's internal knowledge about its stimulatory 'world of action (Merkwelt)', namely the surrounding neural network.

0.3. **Dynamics of cell adhesion and motility.** Cell motility of tissue and blood cells on adhesive substrata is induced through the action of actin filaments, which by organized polymerization and by cross-linking with myosin-II motor proteins constitute a transiently swelling and contracting polymer network that is used by the cell for protrusion in frontal lamellipods, traction force production at the cell-substrate border and subsequent retraction of the rear. This leads to typical two-dimensional picture sequences of adhesion areas $\Omega(t)$ 'beneath the cell' with moving boundaries. For cells moving on an elastic substratum, more descriptive methods have succeeded in estimating the adhesive force vector field in $\Omega(t)$ by solving an inverse problem for the elastic substrate deformation measured at discrete points outside the cell area (see the contribution by D. Ambrosi during this Workshop). However, this methods usually do not consider any modeling of the intracellular biophysical processes causing the motion pattern. Therefore, according to the 'life principle' applied to model supported data analysis in the two preceding examples, we would like to promote the following idea by using the so far developed models of the cytoplasm as a contractile, reactive and highly viscous two-phase flow system, mathematically represented by a hyperbolic-/elliptic system of mass and force balance equations plus a hybrid system of reaction-diffusion-transport equations for the various states of adhesion molecules (integrins), see [3]. The following program would have to be performed: 1.Record the cell geometry by extracting cell outlines $\partial\Omega(t)$ for a picture sequence, 2. simulate actin and integrin dynamics in the given cell geometry $\Omega(t)$, 3. check compatibility of boundary conditions by suitable adjustment of model parameters, and 4. compute the traction forces beneath the cell. For me it still seems a dream to successfully pursue this idea, however, due to joint effort by such or similar modeling approaches we might be able to understand more about the internal biochemical and biophysical regulation mechanisms, which migrating cells use to perform and control their active motility.

References

[1] W. Alt, *150 years – 'Origin of Species', 100 years – concepts 'Gene' and 'Umwelt'. On the role of theory and mathematics, 'dynamics' and 'functions'*, Communications in Mathematical and Theoretical Biology, **11** (2009), 29–30. For downloading see www.esmtb.org

[2] T. Rüting, *Jakob von Uexküll Theoretical Biology, biocybernetics and biosemtiotics*, Communications in Mathematical and Theoretical Biology, **6** (2004), 11–16. For downloading see www.esmtb.org
[3] E. Kuusela and W. Alt, *Continuum model of cell adhesion and migration*, J. Math. Biol., **58** (2009), 135–161.
[4] T. Merkle, M. Rost and W. Alt, *Egocentric path integration models and their application to desert arthopods*, J. Theor. Biology **240** (2006), 385-399.
[5] R. Jolivet, T.J. Lewis and W. Gerstner, *Generalized integrate-and-fire models of neuronal activity approximate spike trains of a detailed model to a high degree of accuracy*, J. Neurophysiol. **92** (2004), 959-976.

An alignment model with double selection mechanism

Ivano Primi
(joint work with Angela Stevens, Juan J.L. Velázquez)

The results of this talk are related to a mathematical model for alignment of elongated cells or filaments in a 2-dimensional geometry. The model is still too simple and abstract to be applied to real alignment phenomena. It has however a very interesting feature, which mirrors a fundamental characteristic of alignment phenomena, namely a dynamics that drives the system from a continuous of orientations into the selection of a finite number of them.

Such a long time dynamics is not an exclusive property of alignment phenomena. A biological population can be often divided in classes according to the values of one or more relevant parameters. In case of alignment phenomena this parameter is the orientation in the space, for age structured populations is the age etc.

Interactions internal to the population or with the external environment can lead to a redistribution of the individuals into the different classes. In several cases the interactions are such that the final effect of this redistribution is the transition from an initial situation, when the individuals are spread more or less randomly over a continuous of classes, to a final situation, when the great majority of the population is split only into a finite number of classes. Often, and this is also the case of alignment phenomena, there is not only selection of a finite number of states but also of a particular distribution of the total population into them.

For two dimensional alignments *exemplo gratia*, if in the long run only two opposite directions are selected, this could mean that one half of the population is oriented along one direction and the other half along the opposite one and no other ways of splitting are possible. Examples of biological relevance for this double selection mechanism could be cell differentiation or plasticity in the hematopoietic stem cell system.

What makes our model for $2D$-alignment relevant, is to be the simplest possible one offering the double selection mechanism, selection of the final states and of the distribution of the population between them.

The basic assumption is that two elongated cells or filaments either attract or repel each other depending on the value of the angular difference between their orientations. If the angle between the filaments or cells is close, then they tend

to align into the same orientation; if the angle between them is larger, then they tend to align themselves in opposite directions. The turning effect is considered to be non-deterministic, which is the main difference with respect to the model presented in [3].

Our model takes the form of an integro-differential equation for a function f on the unit circle $\mathbb{S}^1$:

$$\partial_t f(u,t) = -\int_{\mathbb{S}^1} T[f](u,v) f(u,t)\, dv + \int_{\mathbb{S}^1} T[f](v,u) f(v,t)\, dv\,.$$

Like in kinetic models, f is a density distribution, $f(u,t)$ denotes namely the density distribution of cells or filaments over the orientation $u \in \mathbb{S}^1$ at time t. For practical reasons we have normalized the arc-length of the unit circle to 1 and used the representation $\mathbb{S}^1 = [-1/2, 1/2]$ with identification of the points $1/2$ and $-1/2$.

The first term on the right hand side of the equation describes the bundles of cells or filaments which reorient away from u, the second term the bundles orienting themselves into direction u. From the equation one can easily derive that the total mass $m = \int_{\mathbb{S}^1} f(u)\, du$ is conserved. Up to a scaling it is always possible to set $m = 1$. In this equation T is a turning rate: $T[f](u,v)$ represents, roughly speaking, the probability for a filament oriented along the direction u to re-orient itself in the direction v. Choosing for the turning rate T a simple linear Ansatz with constant interaction rate, one obtains the following definition of T,

$$T[f](u,v) = \int_{\mathbb{S}^1} G_\sigma(v - M_w(u)) f(w,t)\, dw\,.$$

Here G_σ is an even, bounded and periodic probability density, namely the standard periodic Gaussian, which is used to describe the non-deterministic nature of the turning.

The function M_w, the so called optimal reorientation, defines the way the filaments tend to re-orient themselves, depending on their original orientations, due to the interaction with a given filament oriented in the direction w. For a system invariant under rotations $M_w(u) = u + V(w-u)$, where V, the so called orientational angle, is a smooth, 1-periodic and odd function, i.e. $V(-u) = -V(u)$ for all $u \in \mathbb{R}$. Since we assume attraction when the difference $w-u$ is small and repulsion if it is larger, the orientational angle also fulfills the property, $V(z) = V(0) = V(1/2) = 0$, $V(x) > 0$ in $(0,z)$, and $V(x) < 0$ in $(z, 1/2)$ for a suitable $z \in (0, 1/2)$.

The presence of the probability density G_σ allows for non-sharp re-orientations: M_w is the preferred orientation of re-alignment and not the only possible one. A smaller σ means a narrower G_σ and then a higher accuracy of the re-orientation. The limiting case is the Dirac mass $G_0(x) = \delta_0$, which describes deterministic turning. This case has been extensively studied in [3]. In my joint work with Stevens and Velázquez (see [4]) we have looked for steady states in the limit σ positive but small. If we assume that the typical deviation σ and the orientational angle V are small, the evolution equation for the density distribution f can be approximated by a second order parabolic equation using a Fokker-Planck type of

argument, which results in

$$\partial_t f = \frac{\sigma^2 m}{2}\,\partial_{xx} f + \partial_x \left(f(x) \int_{\mathbb{S}^1} V(x-y) f(y) \mathrm{d}y \right) \quad \forall x \in \mathbb{R}\,,$$

where $m = 1$ is the total mass and x has been used in place of u to denote the angle variable. This parabolic equation for $2D$-alignments has been already considered by E. Geigant (see [1]) and by Geigant and Stoll (see [2]), who carried out a bifurcation analysis of steady state solutions and a stability analysis of some of them by means of the Fourier transform. In [4] we concentrate on proving the existence of non constant steady states and on performing a numerical analysis of their stability.

The steady states of the parabolic equation are solutions of

$$\begin{cases} \frac{\sigma^2}{2} f_{xx} + \frac{d}{dx}\left(f(x) \int_{\mathbb{S}^1} V(x-y) f(y) \mathrm{d}y \right) = 0 \quad \forall x \in \mathbb{R} \\ f\left(-1/2\right) = f\left(1/2\right) \\ \int_{\mathbb{S}^1} f(x)\, dx = 1 \end{cases},$$

or equivalently of the first order equation

$$\begin{cases} f_x + f(x) \int_{\mathbb{S}^1} V(x-y) f(y) \mathrm{d}y = 0 \quad \forall x \in \mathbb{R} \\ \int_{\mathbb{S}^1} f(x)\ dx = 1\,. \end{cases}$$

The equivalence between the second- and the first-order formulation is proved by integration/differentiation w.r. to x using that V is 1-periodic and odd. These properties of V allow also to omit the periodicity condition in the first order formulation, since every solution of the first order problem turns out to be 1-periodic. Notice that $f \equiv 1$ is a trivial steady state. In addition, since we are assuming invariance under rotations, every non trivial steady state yields a 1-parameter family of steady states: if f is a non trivial steady state, then any rotation $f_\theta(x) := f(x+\theta)$ of angle $\theta \in (0,1)$ is still a steady state and in general differs from f. The steady state problem has then a strong non-uniqueness property.

If we take $\sigma = 0$ we obtain back the equation studied in [3]:

$$f(x) \int_{\mathbb{S}^1} V(x-y) f(y)\, dy = 0\,.$$

Since $V(0) = V(\pm 1/2) = 0$, every convex combination of a Dirac mass at 0 and a Dirac mass at $\pm 1/2$ is a solution of the last equation. This means that every possible distribution of the total population in two opposite orientations is a steady state and then a possible "limit state" for the solutions of the evolutive equation. For $\sigma = 0$ we have then no mass selection but just selection of the final orientations.

For $\sigma > 0$ this changes: steady states can only be constructed, if the aligning masses are either equal or the total mass is concentrated in one direction. In addition, since for $\sigma > 0$ the evolutive equation is parabolic, the Dirac-deltas steady states are replaced by smooth peak-like density distributions. Type and stability of the steady states depend on the sign of $\mathfrak{I} := \int_0^{1/2} V(x)\, dx$. For a general V this integral is different from zero and its sign has a simple interpretation: if

positive, then the tendency of the filaments to aggregate in one direction is stronger than the one to align in opposite directions, if negative, then the contrary is true.

Therefore it is not surprising that for $\mathfrak{I} < 0$ there is no 1-peak like steady state with the mass strongly concentrated around the orientation $x = 0$. On the contrary, for $\mathfrak{I} > 0$ and under the assumption that σ is "small" with respect to V we could prove existence of a smooth 1-peak like steady state. According to the numerical simulations, this steady state is stable.

A simple heuristic argument allows to understand that, if there is a two-peaks like steady state with concentration of mass around two opposite orientations, then the two peaks must have the same height, i.e. the total population must be equally split between them. The existence of double peaked steady states has been proved both for $\mathfrak{I} > 0$ and for $\mathfrak{I} < 0$. The proof requires, in addition to some technical assumptions on V, the condition that σ is small with respect to V, namely $\sigma < \bar{\sigma}$ for a suitable positive $\bar{\sigma} = \bar{\sigma}(V)$. According to the numerical simulations, what changes with the sign of $\mathfrak{I}$ is the stability of the double peaked steady-states: if the sign is negative they are stable, if it is positive they are unstable. Therefore only if $\mathfrak{I} < 0$ the double peaked steady states can represent possible large time limit behaviors for the solutions of the evolutive equation.

Under suitable assumptions on V and for $\sigma > 0$ sufficiently small it is possible to prove also for $N \geq 3$ the existence of N-peaks like steady states with peaks symmetrically displaced along $\mathbb{S}^1$ and having all the same height. We conjecture that they are all unstable, as it is shown by numerical simulations for the case $N = 4$.

The numerical simulations also show that for $\mathfrak{I} \neq 0$ the trivial steady state $f \equiv 1$ is always unstable, which according to the interpretation of the sign of $\mathfrak{I}$ is not at all surprising.

References

[1] Geigant, E.: *Stability analysis of a peak solution of an orientational aggregation model*, International Conference on Differential Equations, **1, 2** (Berlin, 1999), 1210 - 1216, World Sci. Publ., River Edge, NJ, 2000

[2] Geigant, E.; Stoll M.: *Bifurcation analysis of an orientational aggregation model*, J. Math. Biol. **46** (2003), 537 563

[3] Kang, K.; Perthame, B.; Stevens, A.; Velázquez J.J.L.: *An Integro-Differential Equation Model for Alignment and Orientational Aggregation*, J. Differential Equations **246** (2009), no. 4, 1387 - 1421

[4] Primi, I.; Stevens, A.; Velázquez, J.J.L.: *Mass-Selection in Alignment Models with Non-Deterministic Effects*, Comm. in Partial Differential Equations, **34** (2009), Issue 5, 419 - 456

Asymmetric potentials and motor effect: large deviations and homogenization approaches

Panagiotis Souganidis
(joint work with Benoît Perthame)

In this talk we provide a mathematical analysis for the appearance of concentrations (as Dirac masses) in the solutions to Fokker-Plank systems with asymmetric potentials written as

$$\begin{cases} -\epsilon\frac{\partial^2}{\partial x^2}n_i - \frac{\partial}{\partial x}(\nabla\psi_i(x)\ n_i) + \nu_{ii}n_i = \sum_{j\neq i}\ \nu_{ij}n_j & \text{in } (0,1), \\ \epsilon\frac{\partial}{\partial x}n_i(x) + \nabla\psi_i(x)\ n_i(x) = 0 \quad \text{for } x = 0 \text{ or } 1. \end{cases}$$

or

$$\begin{cases} -\epsilon n^{(1)}_{\epsilon,xx} - (\psi_y(\frac{x}{\epsilon})n^{(1)}_\epsilon)_x + \frac{1}{\epsilon}\nu^{(1)}(\frac{x}{\epsilon})n^{(1)}_\epsilon = \frac{1}{\epsilon}\nu^{(2)}(\frac{x}{\epsilon})n^{(2)}_\epsilon \\ \qquad\qquad\qquad\qquad\qquad\qquad\qquad\qquad\qquad\qquad \text{in } (0,1)\ , \\ -\epsilon n^{(2)}_{\epsilon,xx} + \frac{1}{\epsilon}\nu^{(2)}(\frac{x}{\epsilon})n^{(2)}_\epsilon = \frac{1}{\epsilon}\nu^{(1)}(\frac{x}{\epsilon})n^{(1)}_\epsilon \\ \epsilon n^{(1)}_{\epsilon,x} + \psi_y(\frac{x}{\epsilon})n^{(1)}_\epsilon = n^{(2)}_{\epsilon,x} = 0 \ \text{ for } \ x = 0 \ \text{ or } \ 1\ . \end{cases}$$

These problems have been proposed as models to describe motor proteins moving along molecular filaments. The components of the system describe the densities of the different conformations of the proteins.

Our results are concerned with the limit when ϵ vanishes and are based on the study of a Hamilton-Jacobi equations arising, at the zero diffusion limit, after an exponential transformation change of the phase funxction that yields a semilinear system of viscous Hamilton-Jacobi equations. We consider different classes of conformation transitions coefficients (bounded, unbounded, locally vanishing and oscillating).

Numerical modeling of tumor growth

Thierry Colin
(joint work with Didier Bresch, Frederique Billy, Emmanuel Grenier, Benjamin Ribba, Olivier Saut)

Tumor angiogenesis is a process by which new blood vessels are formed from the existing vas- culature and carry additional nutrients and oxygen to tumor cells, allowing them to proliferate. The process of angiogenesis is extremely important in the development of tumors. It is generally accepted that a tumor, which needs nutrients and oxygen to grow, cannot increase beyond few millimeters cubed without an enhanced blood supply [1]. During tumor growth, a molecular cascade drives the transition from the avascular stage to the vascular stage: new vessels are formed from the surrounding existing vasculature, migrate towards the tumor cells, and pene- trate the tumor mass to deliver oxygen and nutrients to the tumor cells. Indeed, angiogenesis, or new vessel formation, is a result of a complex

molecular balance be- tween numerous pro-angiogenic and anti-angiogenic endogenous substances [2]. The complexity of angiogenesis is partly due to the existence of a number of such factors. In breast cancer for instance, up to seven distinct pro-angiogenic factors can be expressed [3].

Over the last 25 years, several mathematical models of angiogenesis have been developed (see [4] for a review). Discrete mathematical models, based on cellular automata, have been mainly used to predict the structure of extra- and intratumoral vascular networks. Continuous models of tumor-induced angiogenesis are based on ordinary or partial differential equations governing the change in endothelial cell density, and the concentrations of tumor pro-angiogenic factors and of fibronectin (a component of the extra-cellular matrix). From the physical point of view, these models focus mainly on the endothelial cell diffusion, chemotaxis and haptotaxis. It has also been proposed that mathematical models of angiogenesis can be coupled with those of tumor growth. In [5], X. Zheng, S. M. Wise, and V. Cristini propose a vascular tumor growth model in which the tumor growth model proposed by H. M. Byrne and M. A. Chaplain [6] is coupled with a continuous-discrete model of angiogenesis, such as that described by A. R. Anderson and M. A. Chaplain [7]. In [8], P. Macklin et al. couple a tumor growth model with a discrete model of tumor-induced an- giogenesis in order to take into account the impact of blood flow on changes in the vascular network. Due to their complexity, these models are only qualitative. Moreover, they only integrate one or two of the molecular factors that drive the angiogenesis process, and the underlying tumor growth model is often very simplistic and fails to take cell cycle regulation into account.

Since the angiogenesis process was first identified as a key process in tumor development a few years ago, pharmaceutical companies have been looking for inhibitors of angiogenesis. Several anti- angiogenic molecules have been identified and tested in clinical trials but, with a few exceptions, and as is all too often the case with targeted therapies, efficacy has been difficult to demonstrate. This makes it rather difficult to assess attempts to optimize treatment. New anti-cancer drugs are designed to target a particular cancer process, unlike standard chemotherapeutic compounds that have a cytotoxic effect on all proliferative cells. Targeted therapies, which are also known as cytostatic treatments act mainly at the molecular level. For instance, some anti-angiogenic drugs, such as the best known, Bevacizumab (Avastin, Roche), prevent the binding of vascular endothelial growth factor (VEGF), a pro-angiogenic endogenous substance, to Flk-1 receptors located on the membrane of endothelial cells that constitute the blood vessels. This results in the inhibition of endothelial cell proliferation and, in consequence, of the formation of new blood vessels, without any direct toxic effect on healthy cells. To make it possible to analyze the effect of such molecular-targeted treatments by means of mathematical models, we need to include the main molecular entities in multiscale models of tumor growth. In this paper we describe a pharmacologically-based continuous mathematical model of an- giogenesis and tumor growth. At the

molecular level, we were careful to use pharmacological laws to model the activation of angiogenesis as the result of the binding of ma jor angiogenic molecular substances to their respective receptors. This molecular-level model was embedded in the macroscopic model, based on reaction-diffusion partial differential equations, that describes the spatio-temporal change in the densities of the unstable and stable endothelial cells that constitute the blood vessel wall. At each of the time steps in the model, sources of oxygen were defined according to the spatial disposition of the endothelial cells. The oxygen concentration was then computed, and introduced as an input signal into the cell cycle model of tumor cells. Indeed, depending on the local con- centration of oxygen, we assumed that cancer cells would proliferate, die, or enter the quiescent compartment. In the model, quiescent cells, deprived of oxygen, secrete vascular endothelial growth factor (VEGF). This in turn activates angiogenesis, and this constitutes the feedback loop of the model.

References

[1] Folkman, J., Jan, *What is the evidence that tumors are angiogenesis dependent?* J Natl Cancer Inst **82** (1), (1990) 46.

[2] Hanahan, D., Folkman, J., *Patterns and emerging mechanisms of the angiogenic switch during tumorigenesis*, Cell **86** (3), (1996) 353364.

[3] Relf, M., LeJeune, S., Scott, P. A., Fox, S., Smith, K., Leek, R., Moghaddam, A., Whitehouse, R., Bicknell, R., Harris, A. L., *Expression of the angiogenic factors vascular endothelial cell growth factor, acidic and basic fibroblast growth factor, tumor growth factor beta-1, platelet- derived endothelial cell growth factor, placenta growth factor, and pleiotrophin in human primary breast cancer and its relation to angiogenesis*, Cancer Res **57** (5), (1997) 963969.

[4] Mantzaris, N. V., Webb, S., Othmer, H. G., *Mathematical modeling of tumor-induced angiogenesis*, J Math Biol **49** (2), (2004) 111187.

[5] Zheng, X., Wise, S. M., Cristini, V., *Nonlinear simulation of tumor necrosis, neo- vascularization and tissue invasion via an adaptive finite-element/level-set method*, Bull Math Biol **67** (2), (2005) 211259.

[6] Byrne, H. M., Chaplain, M. A., *Growth of necrotic tumors in the presence and absence of inhibitors*, Math Biosci **135** (15), (1996) 187216.

[7] Anderson, A. R., Chaplain, M. A., *Continuous and discrete mathematical models of tumor-induced angiogenesis*, Bull Math Biol **60** (5), (1998) 857899.

[8] Macklin, P., McDougall, S., Anderson, A. R. A., Chaplain, M. A. J., Cristini, V., Lowengrub, J., *Multiscale modelling and nonlinear simulation of vascular tumour growth*, J Math Biol **58** (4-5), (2009) 765798.

The random walk of Azospirillum brasilense

K.P. Hadeler

(joint work with Kevin Flores)

In the last few years we have been interested in modeling dynamics where different phases are coupled by random transitions. One example is coupling an active phase to a quiescent phase which generally stabilizes the active dynamics (in the case of equal coupling rates [4]) but may also produce Turing-like instabilities (sufficiently

distinct coupling rates [5] [3] [6]). We refer to the review paper [7] for applications of these ideas to spread in space and biological problems. Another class of problems are random walks with alternating modes of motion. Two examples of the latter class are described here in detail [1] [2].

The free-living bacterium *Azospirillum brasilense* shows a mixed pattern of propagation. In liquid medium it has one polar flagellum and it moves forward and backward on a straight line while the direction of this line changes only slowly. The motion of the bacterium has been modeled by a system of two transport equations in R^3 which are based on a biased correlated random walk for the forward/backward motion and diffusion on the unit sphere for the change of direction. State variables are position, direction and forward/backward, hence time-dependent solutions arefunctions of a variable in $R_+ \times R^3 \times S^2 \times \{\pm\}$. Parameters are speeds, turning rates, diffusion rates which depend on whether motion is forward or backward. For this system a diffusion approximation has been derived. The diffusion coefficient is a positively definite quadratic form in the speeds with coefficients depending on turning and diffusion rates on the sphere. The formula shows clearly how the convection term of the 1D biased correlated random walk yields a large contribution to the 3D diffusion coefficient. Similar results have been obtained for the 2D problem (which is not simply the restriction of the 3D problem to two dimensions).

The method of proof is moment approximation, closure and Kac' trick of elimination of assistant variables. The methods have also been used to describe the random motion on circles of whirligig beetles in which case the diffusion coefficient depends on speed, turning rate and radius of the circles.

References

[1] K. Flores, K.P. Hadeler,
The random walk of Azospirillum brasilense, J. Biol. Dynamics, March 2009

[2] K.P. Hadeler, *The Walk of the Whirligig* mscr. 2009

[3] L. Bilinsky, K.P. Hadeler, *Quiescence stabilizes predator-prey relations*, J. Biol. Dynamics **3** (2008), 196–208

[4] K.P. Hadeler, T. Hillen, *Coupled dynamics and quiescent states*,Math Everywhere, 7–23, Springer, Berlin, 2007

[5] K.P. Hadeler, *Quiescent phases and stability*, Linear Algebra Appl. **428** (2008), 1620–1627

[6] K.P. Hadeler, *Homogeneous systems with a quiescent phase*,
Math. Model. Nat. Phenom. **3** (2008), 115–125

[7] K.P. Hadeler, T. Hillen, M. Lewis, *Biological Modeling with Quiescent Phases*, Chapter 5 in "Spatial Ecology", S. Cantrell, C. Cosner, S. Ruan (eds), 2009

Progressive fronts in several biological problems

Guillemette Chapuisat

Many biological problems are modeled by a progressive front solution of a reaction-diffusion equation. The spreading direction may be due to the geometry of the space but it can also be forced by the non linearity. For example, a depolarization wave during ischemic stroke follows a reaction-diffusion mechanism in the gray

matter and a diffusion and absorption equation in the white matter, but the gray matter is only a thin layer at the periphery of the brain. Hence depolarization waves are solutions of

$$\frac{\partial u}{\partial t} - \triangle u = \lambda u(u-\theta)(1-u)1_{\Omega} - \alpha u 1_{\mathbb{R}^n \setminus \Omega} \tag{1}$$

where Ω is a domain that represents the gray matter, a cylinder for example. I have studied the existence of travelling front for such an equation using energy methods.

In population dynamics, there are equations of the same type. For example, if f is the density of a population that depends on the time t, the space $x \in \mathbb{R}$ and on a quantitative trait $y \in \mathbb{R}$ and if the most adapted trait is $y = 0$ after some simplifications, f is a solution of the equation

$$\frac{\partial u}{\partial t} - \triangle u = \lambda u(1-u) - \alpha |y|^2 u. \tag{2}$$

With H. Berestycki, I have proved that this equation has a travelling front solution if and only if α is small enough. We use moving planes methods.

Another problem of the same type appears in the modelling of tumour cords (i.e. tumors that grow along a blood vessel).

Influence of habitat fragmentation on species persistence and biological invasions

François Hamel

(joint work with Henri Berestycki and Lionel Roques)

The talk is concerned with the mathematical analysis of some aspects of species persistence and biological invasions in heterogeneous diffusive excitable media. Reaction-diffusion equations offer a very rich structure from a mathematical point of view and, even oversimplified, they provide qualitative estimates which may help to get a better understanding of the underlying biological models. The model which we have studied is based on the patch model borrowed from a book by Shigesada and Kawasaki (*Biological Invasions, Theory and Practice*, Oxford Univ. Press, 1997). It describes the evolution of a (scalar) quantity u, the density of a species, in a periodic excitable medium. The function u satisfies the reaction-diffusion equation

$$\frac{\partial u}{\partial t} - \nabla \cdot (A(x)\nabla u) = f(x,u), \quad x \in \mathbb{R}^N,$$

where the diffusion A and the reaction term f are assumed to be periodic in x. The growth rate, namely the derivative $f'_u(x,0)$ of $f(x,u)$ at $u = 0$, may change sign as x varies. But f is assumed to satisfy $f(x,0) = 0$ and $f(x,u)/u$ is decreasing with $u > 0$ and is nonpositive when u is large, uniformly in x. Typical examples are $f(x,u) = (\mu(x) - \nu(x)u)u$, where μ and ν are periodic and continuous, and ν is

positive. We have given a necessary and sufficient condition for species persistence, that is for the existence of positive solutions $p(x)$ of the stationary problem

$$-\nabla \cdot (A(x)\nabla p) = f(x,p) \ \text{ in } \mathbb{R}^N.$$

The existence, and uniqueness, of p is shown to be equivalent to the negativity of the principal periodic eigenvalue of the linearized operator $-\nabla \cdot (A(x)\nabla) - f'_u(x,0)$ around 0 (the state 0 is then unstable). We have then proved new Liouville type results for these semilinear elliptic equations with periodic coefficients, by using sliding methods and subsolutions which are constructed in large enough balls. We have also studied the influence of the size and the location of the heterogeneities in the medium. We have especially shown the negative effect of the fragmentation on species persistence (environmental fragmentation, which is mainly due to human activities and geographical barriers, is known to be one of the causes for species endangerment and loss of biodiversity). The proofs, which are based on periodic rearrangement inequalities, give in particular a rigorous justification, as well as a generalization in a much more general framework, to some formal results obtained by Shigesada and Kawasaki. Then, we have proved that the condition for species persistence is equivalent to the condition for biological invasions, that is the existence of pulsating traveling fronts connecting the unstable state 0 to the unique positive stationary state p. A formula for the minimal speed of propagation in each direction has been given. Lastly, I have talked about the following optimization problem: in a binary environment where the growth rate $f'_u(x,0)$ takes only two values with a given average and where the diffusion reduces to the Laplace operator, how to maximize the chances for species survival ? From a mathematical point of view, this means minimizing the principal periodic eigenvalue of an elliptic operator, when the potential takes only two values and has a given average. The unknowns are the locations of the two regions, say favourable and unfavourable, of the medium in each cell of periodicity. We have obtained numerical and rigorous results on this shape optimization problem. There seems to be two main types of optimal configurations: the ball-shaped and the stripe-shaped configurations, depending on the size of favourable regions. However, we have proved that each of these two configurations is not always optimal and shown that the optimal configurations reflect a compromise between the detrimental habitat edge effects and the positive advantage of the domain boundary effects (proximity of habitat in the neighbour cells).

References

[1] H. Berestycki, F. Hamel, L. Roques, *Analysis of the periodically fragmented environment model : I – Species persistence*, J. Math. Biology **51** (2005), 75–113.

[2] H. Berestycki, F. Hamel, L. Roques, *Analysis of the periodically fragmented environment model : II – Biological invasions and pulsating travelling fronts*, J. Math. Pures Appl. **84** (2005), 1101–1146.

[3] L. Roques, F. Hamel, *Mathematical analysis of the optimal habitat configurations for species persistence*, Math. Biosciences **210** (2007), 34–59.

Deterministic and stochastic aspects of recombination

Ellen Baake
(joint work with Michael Baake, Inke Herms)

Populations evolving under the joint influence of recombination and resampling (traditionally known as genetic drift) are investigated. First, we summarise and adapt a deterministic approach, as valid for infinite populations, which assumes continuous time and single crossover events [1]. The corresponding nonlinear system of differential equations permits a closed solution, both in terms of the type frequencies and via linkage disequilibria of all orders; we point out that this is due to some 'hidden' linearity in the model. To include stochastic effects, we then consider the corresponding finite-population model, the Moran model with single crossovers, and examine it both analytically and by means of simulations [2]. Particular emphasis is on the connection with the deterministic solution. If there is only recombination and every pair of recombined offspring replaces their pair of parents (i.e., there is no resampling), then the *expected* type frequencies in the finite population, of arbitrary size, equal the type frequencies in the infinite population. This is a very unusual property for a stochastic process with interaction, which may be traced back to conditional independence of certain marginal processes. If resampling is included, the stochastic process converges, in the infinite-population limit, to the deterministic dynamics, which turns out to be a good approximation already for populations of moderate size.

References

[1] M. Baake, E. Baake, *An exactly solved model for recombination, mutation and selection* <http://www.TechFak.Uni-Bielefeld.DE/ags/bm/preprints/revreco7.ps.gz> Can. J. Math. **55** (2003), 3-41.

[2] E. Baake, I. Herms, *Single-crossover dynamics: finite versus infinite populations* <http://www.techfak.uni-bielefeld.de/ags/bm/preprints/moreco.pdf> Bull. Math. Biol. **70** (2008), 603-624

Lipschitz semigroups on metric spaces and structural stability of a nonlinear population model

Piotr Gwiazda
(joint work with Anna Marciniak-Czochra)

Models describing time evolution of physiologically structured populations have been extensively studied in recent years, eg. Ref.[3, 8, 6]. Global existence and structural stability of structured models were established for solutions defined in Banach space L^1 [6, 8]. However, in biological applications, it is often necessary to describe populations in which the initial distribution of the individuals is concentrated with respect to the structure and it is relevant to consider initial data in

the space of Radon measures as proposed in [7]. The model has the general form,

$$\begin{aligned} \partial_t \mu_t + \partial_x (F_2(\mu_t)\mu_t) &= F_3(\mu_t)\mu_t, \quad \text{in } \mathbb{R}^+ \times [0,T], \\ F_2(\mu_t)(0)\ \mu_t(0) &= \int_{\mathbb{R}}^{+} F_1(\mu_t)(x)\ d\mu_t(x), \quad \text{in } [0,T], \end{aligned} \tag{1}$$

where x denotes the state of an individual (for example the size, level of neoplastic transformation, stage of differentiation) and $u(x,t)$ the density of individuals being in state $x \in \mathbb{R}^+$ at time t. By $F_3(u,x)$ we denote a function describing the individual's rate of evolution, such as the growth or death rate. $F_2(u,x)$ describes the rate of the dynamics of the structure, i.e., the dynamics of the transformation of the individual state. The boundary term describes the influx of new individuals at state $x = 0$. The example of nonlinear functions F_1, F_2, and F_3 is $F_i \colon \mathcal{M}(\mathbb{R}^+) \to W^{1,\infty}(\mathbb{R}^+)$, $F_i(\mu_t)(x) = f(x)G\left(\int_0^\infty \varphi d\mu_t\right)$ with $f \in W^{1,\infty}$, G - Lipschitz continuous, $\varphi \in W^{1,\infty}$.

For linear age-dependent population dynamics, a qualitative theory using semigroup methods and spectral analysis has been laid out in [4]. The follow-up works (see e.g. Ref. [3]) are devoted to nonlinear models. All the results there concerning continuous dependence of solutions on time and initial state are based on the weak$*$ topology of Radon measures. There exist simple counter-examples indicating that continuous dependence, either with respect to time or to initial state, generally cannot be expected in the strong topology.

The aim of this study is to consider such system of equations as the Lipschitz semigroup on metric space. In fact we are motivated by the results from the kinetic theory where the application of the so-called bounded Lipschitz distance and Wasserstein distance to transport type equation have been known for many years (see e.g. [2]). We will consider two different metrics:

1. Flat metric (also called: bounded Lipschitz distance)

We look for a metric defined on the space $\mathcal{M}^+(\mathbb{R}^+)$. For $\mu, \nu \in \mathcal{M}^+(\mathbb{R}^+)$ the flat metric ρ is defined by

$$\rho_(\mu,\ \nu) \quad := \quad \sup\ \left\{ \int_{\mathbb{R}^+}\ \psi\, d(\mu - \nu) \ \middle|\ \|\psi\|_{W^{1,\infty}} \le 1 \right\}.$$

Observe that

$$\rho_F(\mu,\ \nu) \le |\mu - \nu|(\mathbb{R}^+) \le \mu(\mathbb{R}^+) + \nu(\mathbb{R}^+) < \infty.$$

Lemma: *The set $\mathcal{M}^+(\mathbb{R}^+)$ endowed with the flat metric ρ_F is a complete separable metric space.*

2. Wasserstein-like metric

Metric for the space $\mathcal{M}_1^+(\mathbb{R}^+)$ (finite nonnegative measures, first moment integrable). For $\mu, \nu \in \mathcal{M}_1^+(\mathbb{R}^+)$ the metric ρ_W is defined by

$$\rho_W(\mu,\nu) := \sup \left\{ \int_{\mathbb{R}^+} \psi d(\mu - \nu) \middle|\ \|\psi'\|_{L^\infty} \le 1,\ |\psi(\cdot)| \le 1 + |\cdot| \right\}.$$

Observe that

$$\rho_W(\mu,\ \nu) \le \int_{\mathbb{R}^+} (1+x) d\mu + \int_{\mathbb{R}^+} (1+x) d\nu < \infty.$$

Lemma *The set $\mathcal{M}_1^+(\mathbb{R}^+)$ endowed with the flat Wasserstein-like ρ_W is a complete separable metric space.*

Remark: To indicate the difference between flat metric and Wasserstein-like metric let us consider the distance w.r.t. both metrics of two Dirac measures located at the points a and b. We compute directly:

$$\rho_F(\delta_a, \delta_b) = \min\{2, |a-b|\}$$

and

$$\rho_W(\delta_a, \delta_b) = |a-b|$$

Let us formulate the main result:

Theorem (Existence and Lipschitz dependence on model ingredients)
Suppose that $F, \tilde{F} : \mathcal{M}^+(\mathbb{R}^+) \to \left\{(a,b,c) \in W^{1,\infty}(\mathbb{R}^+)^3 \mid b(0) > 0,\ a \geq 0\right\}$

(i) $\sup_{\mu\in\mathcal{M}^+(\mathbb{R}^+)} \|F(\mu)\|_{W^{1,\infty}} < \infty$ *and*
$\sup_{\mu\in\mathcal{M}^+(\mathbb{R}^+)} \|\tilde{F}(\mu)\|_{W^{1,\infty}} < \infty$,

(ii) *for any $R > 0$, there exist constants $L_R, \tilde{L}_R > 0$ such that*
$\|F(\mu) - F(\nu)\|_\infty \leq L_R\, \rho_F(\mu,\nu)$ *and*
$\|\tilde{F}(\mu) - \tilde{F}(\nu)\|_\infty \leq \tilde{L}_R\, \rho_F(\mu,\nu)$
for all $\mu, \nu \in \mathcal{M}^+(\mathbb{R}^+)$ with $|\mu|(\mathbb{R}^+), |\nu|(\mathbb{R}^+) \leq R$.

Then, for any initial measure $\mu_0 \in \mathcal{M}^+(\mathbb{R}^+)$, there exists a Lipschitz continuous solution $\mu : [0,T[\longrightarrow (\mathcal{M}^+(\mathbb{R}^+), \rho_F)$. Moreover, the solutions satisfy

(1) $\rho_F(\mu_t, \mu_s) \leq C_1|t-s|$,

(2) $\rho_F(\mu_t^{F_1,F_2,F_3}, \nu_t^{\tilde{F}_1,\tilde{F}_2,\tilde{F}_3})$
$\leq e^{C_2 t} \cdot \rho_F(\mu_0,\nu_0) + C_3 t \cdot (\|F_1 - \tilde{F}_1\|_\infty + \|F_2 - \tilde{F}_2\|_\infty + \|F_3 - \tilde{F}_3\|_\infty)$
where C_1, C_2 and C_3 are some positive constants, and $\mu_t^{F_1,F_2,F_3}$, $\nu_t^{\tilde{F}_1,\tilde{F}_2,\tilde{F}_3}$ are two solutions for initial conditions μ_0 and ν_0 and kinetics $F = (F_1,F_2,F_3)$ and $\tilde{F} = (\tilde{F}_1,\tilde{F}_2,\tilde{F}_3)$, respectively.

Remark: The same result holds for Wasserstein-like metric with additional assumption $\sup_{\mu\in\mathcal{M}_1^+(\mathbb{R}^+)} \|\partial_x F_3(\mu)\|_{L^\infty_{1+x}} < \infty$ bounded.

Remark: In the proof of the above theorem the estimates for linear problem based on dual problem are essential. For different applications of the dual formula to structure population model see [9].

Remark: Contrary to the previous paper [5], where the proof of the existence was done by showing the compactness with help of mutational equations (see: [1]) in the present work we use simpler idea of Lipschitz semigroups on metric spaces. That provides the much shorter proof and possibility to construct effective numerical approximation.

The last issue that we would like to discuss is the question of the proper distance that should be taken into account in such a problem. It is close to the problem of *empirical stability*. For the comparison of the model with the "experiment" and callibration, one can ask: What is the usual information from "experiments"?

$$\left\{\int_{nh}^{(n+1)h} d\mu\right\}_{n=1}^{\infty} = \{a_n\}_{n=1}^{\infty} \quad \text{(discrete aggregated information)}.$$

Assume that $\{a_n\}_{n=1}^{\infty}$ is given and define

$$A = \{\mu \in \mathcal{M}^+(\mathbb{R}^+) \mid \int_{nh}^{(n+1)h} d\mu = a_n, n = 1, 2, \ldots\}.$$

What is diam(A)? How it depends on h?

- For norm metric it does not depend on h, and $\operatorname{diam}_{\|\cdot\|_{\mathcal{M}(\mathbb{R})}}(A) = 2\sum_{n=1}^{\infty} a_n$.
- The same if we consider $\operatorname{diam}_{\|\cdot\|_{L^1}}(A \cap L^1) = 2\sum_{n=1}^{\infty} a_n$.

- For the metric ϱ_F we have $\operatorname{diam}_{\varrho_F}(A) \leq \min\{h, 2\}\sum_{n=1}^{\infty} a_n$.
- For the metric ϱ_W we have $\operatorname{diam}_{\varrho_W}(A) \leq h\sum_{n=1}^{\infty} a_n$.

References

[1] Aubin, J.-P. (1999): *Mutational and Morphological Analysis : Tools for Shape Evolution and Morphogenesis*, Birkhäuser-Verlag, Systems and Control: Foundations and Applications

[2] Cedric Villani (2003): Topics in optimal transportation, AMS

[3] Diekmann O. and Getto P. (2005) Boundedness, global existence and continuous dependence for nonlinear dynamical systems describing physiologically structured populations. *J. Differ. Equations* **215:** 268–319.

[4] Diekmann O., Gyllenberg M, Metz J.A.J., Thieme H.R. (1998): On the formulation and analysis of general deterministic structured population models: I. Linear theory, *J. Math. Biol.* **36**, pp. 349–388.

[5] Gwiazda P., Lorenz T. and Marciniak-Czochra A. (2008) Flat metric and structural stability of a nonlinear population model. Submitted

[6] Iannelli M. (1995) *Mathematical Theory of Age-Structured Population Dynamics*, Applied Math. Monographs, CNR, Giardini Editori e Stampatori in Pisa.

[7] Metz J.A.J. and Diekmann O. (1986): *The Dynamics of Physiologically Structured Populations*, Springer, Lecture Notes in Biomathematics, vol. 68

[8] Webb G.F. (1985) *Nonlinear Age-Dependent Population Dynamics*, Dekker.

[9] Perthame B. (2007): Transport equations in biology Birkhäuser.

Reporter: Thomas Lepoutre

Participants

Prof. Dr. Wolfgang Alt
Institut für zelluläre & molekulare
Botanik (IZMB), Theoret. Biologie
Universität Bonn
Kirschallee 1
53115 Bonn

Prof. Dr. Davide Ambrosi
Dipartimento di Matematica
Politecnico di Milano
Piazza Leonardo da Vinci, 32
I-20133 Milano

Prof. Dr. Ellen Baake
Technische Fakultät
Universität Bielefeld
Universitätsstr. 25
33615 Bielefeld

Dr. Thomas Blesgen
Max-Planck-Institut für Mathematik
in den Naturwissenschaften
Inselstr. 22 - 26
04103 Leipzig

Ansgar Bohmann
Universität Heidelberg
Angewandte Mathematik und Bioquant
Im Neuenheimer Feld 267
69120 Heidelberg

Prof. Dr. Jose A. Carrillo
Departament de Matematiques
Universitat Autonoma de Barcelona
Edifici C
E-08193 Bellaterra (Barcelona)

Dr. Guillemette Chapuisat
LATP(Mathematiques)
Faculte St. Jerome
Universite Aix-Marseille III
Avenue Escadrille Normandie-N.
F-13397 Marseille Cedex 20

Prof. Dr. Thierry Colin
Mathematiques et Informatique
Universite Bordeaux I
351, cours de la Liberation
F-33405 Talence Cedex

Prof. Dr. Andras Czirok
Dept. of Cell Biology & Anatomy
University of Kansas Med. Ctr.
1008 WHW 3901 Rainbow Blvd.
Kansas City KS 66160-7400
USA

Prof. Dr. Emmanuele DiBenedetto
Vanderbilt University
Department of Mathematics
1416 Stevenson Center
Nashville , TN 37240
USA

Prof. Dr. Odo Diekmann
Department of Mathematics
Utrecht University
Budapestlaan 6
NL-3584 CD Utrecht

Dr. Marie Doumic-Jauffret
INRIA Rocquencourt
Domaine de Voluceau
B. P. 105
F-78153 Le Chesnay Cedex

Prof. Dr. Messoud Efendiyev
Institut für Biomathematik
und Biometrie
GSF Forschungszentrum Neuherberg
Ingolstädter Landstr. 1
85764 Neuherberg

Prof. Dr. Heinrich Freistühler
Fachbereich Mathematik u. Statistik
Universität Konstanz
Universitätsstr. 10
78457 Konstanz

Jan Fuhrmann
Universität Heidelberg
Angewandte Mathematik und Bioquant
Im Neuenheimer Feld 267
69120 Heidelberg

Dr. Pierre Gabriel
Universite Pierre et Marie Curie
BC 187
4, Place Jussieu
F-75252 Paris Cedex 05

Scott Gruver
Vanderbilt University
Department of Pharmacology
RRB
23rd Ave. Pierce
Nashville , TN 37232
USA

Prof. Dr. Piotr Gwiazda
Institute of Applied Mathematics
Warsaw University
ul. Banacha 2
02-097 Warsaw
POLAND

Prof. Dr. Mats Gyllenberg
Department of Mathematics
and Statistics
University of Helsinki
P.O. 68
FIN-00014 University of Helsinki

Prof. Dr. Karl Peter Hadeler
Mathematisches Institut
Universität Tübingen
Auf der Morgenstelle 10
72076 Tübingen

Prof. Dr. Francois Hamel
LATP(Mathematiques)
Faculte St. Jerome
Universite Aix-Marseille III
Avenue Escadrille Normandie-N.
F-13397 Marseille Cedex 20

PD Dr. Dirk Horstmann
Mathematisches Institut
Universität zu Köln
Weyertal 86 - 90
50931 Köln

Prof. Dr. Dr.h.c. Willi Jäger
Institut für Angewandte Mathematik
Universität Heidelberg
Im Neuenheimer Feld 294
69120 Heidelberg

Prof. Dr. Kyungkeun Kang
Department of Mathematics
Sungkyunkwan University
Cheoncheon-dong 300
Suwon 440-746
Republic of Korea

Anita Kettemann
Fachbereich Mathematik
Universität Stuttgart
Pfaffenwaldring 57
70569 Stuttgart

Prof. Dr. Markus Kirkilionis
Mathematics Institute
University of Warwick
Gibbet Hill Road
GB-Coventry CV4 7AL

Dr. Thomas Lepoutre
Universite Pierre et Marie Curie
BC 187
4, Place Jussieu
F-75252 Paris Cedex 05

Prof. Dr. Michael C. Mackey
Centre for Nonlinear Dynamics
Department of Physiology
McGill University
3655 Prom. Sir William Osler
Montreal Quebec H3G 1Y6
CANADA

Dr. Anna Marciniak-Czochra
Institut für Angewandte Mathematik
Universität Heidelberg
Im Neuenheimer Feld 294
69120 Heidelberg

Dr. Sepideh Mirrahimi
Universite Pierre et Marie Curie
BC 187
4, Place Jussieu
F-75252 Paris Cedex 05

Prof. Dr. Jeremi Mizerski
Interdisciplinary Centre for Mathematics
and Computational Modelling ICM
University of Warsaw
Pawinskiego 5a
02-106 Warsaw
POLAND

Prof. Dr. Johannes Müller
Zentrum Mathematik
TU München
Boltzmannstr. 3
85748 Garching bei München

Prof. Dr. Giovanni Naldi
Dipartimento di Matematica
Universita di Milano
Via C. Saldini, 50
I-20133 Milano

Dr. Maria Neuss-Radu
Institut für Angewandte Mathematik
Universität Heidelberg
Im Neuenheimer Feld 294
69120 Heidelberg

Prof. Dr. Hans G. Othmer
School of Mathematics
University of Minnesota
270A Vincent Hall
625-9845
Minneapolis , MN 55455
USA

Prof. Dr. Benoit Perthame
Universite Pierre et Marie Curie
BC 187
4, Place Jussieu
F-75252 Paris Cedex 05

Dr. Ivano Primi
Universität Heidelberg
Angewandte Mathematik und Bioquant
Im Neuenheimer Feld 267
69120 Heidelberg

Dr. Gael Raoul
Centre de Mathématiques et de Leurs
Applications (CMLA)
Ecole Normale Superieure de Cachan
61, Avenue du President Wilson
F-94235 Cachan Cedex

Prof. Dr. Andrea A. Robitzki
Universität Leipzig
Center of Biotechnology and Biomedicine
(BBZ)
Deutscher Platz 5
04103 Leipzig

Dr. Matthias Röger
Hausdorff Center for Mathematics
& Institute for Applied Mathematics
Universität Bonn
Endenicher Allee 60
53115 Bonn

Prof. Dr. Christian Schmeiser
Fakultät für Mathematik
Universität Wien
Nordbergstr. 15
A-1090 Wien

Dr. Bernd Schmidt
Zentrum Mathematik
Technische Universität München
85747 Garching bei München

Prof. Dr. Panagiotis E. Souganidis
Department of Mathematics
The University of Chicago
1118 E 58th St., University Ave.
Chicago IL 60637
USA

Prof. Dr. Angela Stevens
Universität Heidelberg
Angewandte Mathematik und Bioquant
Im Neuenheimer Feld 267
69120 Heidelberg

Sebastian Streichan
EMBL Heidelberg
Meyerhofstr. 1
69117 Heidelberg

Prof. Dr. Juan J. L. Velazquez
Instituto Ciencias Matematicas (ICMAT)
Universidad Complutense
Plaza de Ciencias 3
E-28040 Madrid

Prof. Dr. Cornelis Weijer
School of Life Sciences
University of Dundee
MSI/WTB Complex
Dow Street
GB-Dundee DD1 5EH